8 Ground-Based Remote Sensing Systems

A traditional approach to introduce remote sensing systems is to group them into two categories, namely passive and active systems. In passive remote sensing the equipment used to acquire the information from the target (object under study) gathers the data from the **natural energy** emitted and/or reflected by the target. The measuring system described in Sections (4.7.6) and (4.7.7) can be considered a kind of passive remote system. In active remote sensing, instead, the measuring system **emits energy** that "illuminates" the target, and receives part of **its own energy** reflected or scattered by the target (Lillesand et al., 2004). In both cases the energy arriving from the target is analyzed to draw information about the characteristics of the target (velocity, position, size, temperature, aerosol, etc.).

Remote sensing can be performed in different media: solid, fluid or vacuum. Acoustic systems used for measuring flow, as those presented in Section (5.4.4.), could be considered remote sensing systems in a fluid (water) where the sensing wave is a sound wave. Other systems use electromagnetic waves in air, as in the case of radar, or in a physical solid medium such as in fiber optic or soil; an example of the last method is called **Distributed Temperature Sensing** (**DTS**) and will be described below.

In this chapter we will pay attention to active remote sensing systems, where energy is irradiated from the measuring systems to the target, the propagating wave being either electromagnetic or acoustic.

8.1 Distributed Temperature Sensing (DTS)

8.1.1 Introduction

In the near past, thermal hydrological processes have been studied using point measurements, as can be obtained from thermocouples, thermistors and Integrated Circuit sensors (I.C.). In the last few years, a very interesting system with unique characteristics for measuring temperature in environmental sciences and industrial applications has emerged (Selker et al., 2006). It permits the temperature of thousands of points to be simultaneously monitored, which could reveal interactions and processes yet unknown.

This technology is based on the use of fiber optics (f.o.) as sensors and allows environmental processes to be continuously studied over a much greater spatial scale than has been done until now. The measuring of temperature and pressure in laboratory conditions by means of f.o. is not new, but the methods to obtain the information from f.o. sensors and the portability of the instruments have evolved in the last years. These advances have made it possible to use these new tools in field conditions (Selker et al., 2006).

In order to introduce the measuring principles that have been reported as most adequate for environmental applications, it is necessary to explain what f.o. are and how they are employed by the different methods for measuring temperature.

8.1.2 Optical Fibers

Optical fibers are flexible filaments of circular section made of glass or plastic which are barely thicker than a hair. They have an internal transparent core surrounded by a layer of material of lower refractive index. This difference in indexes causes total internal reflection of the light, making the fiber behave as a waveguide.

Because light is confined to the core, which permits light to be transmitted between the two ends of the fiber, they are commonly called "light pipes". The external layer, also called cladding material, is surrounded by a protective coating made of a polymer (Fig. 8.1).

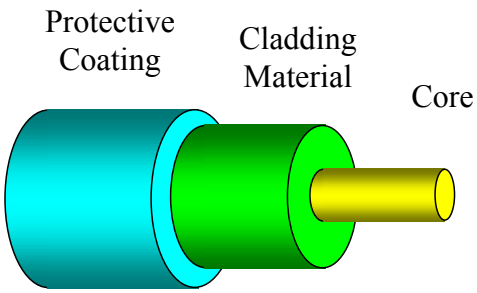

Fig. 8.1: Fiber optic components.

Fiber optics are capable of transmitting high bandwidths over long distances with low losses, and is not interfered by electromagnetic noise. For these reasons they are replacing copper wires in local area data transmission networks and are of great importance in transoceanic communications.

8.1.3 Bragg Grating

Usually, in a f.o. used for communications, it is desired that the light passes through the fiber without internal scattering; the core is thus made as uniform as possible along its length. But when the f.o. is used as a sensor, it may be desired to introduce some periodical variation of the refractive index of the core along the length of the

fiber to obtain a Bragg grating. It has been mentioned in Section (3.5.1) that the Bragg law is valid for electromagnetic waves, as is the case of light propagating in f.o.

The Bragg scattering law gives the conditions for the backscattered light to interfere constructively and permits the f.o. to be used as a sensor. Therefore, the refractive index of the core is increased by design at regular intervals d (Fig. 8.2), where d is an integer number (n) of half-wavelengths of the light (λ) that is desired to be backscattered, i.e.,

$$d = n\frac{\lambda}{2} \qquad n = 1, 2, 3, \ldots \tag{8.1}$$

By measuring the wavelength of the scatters it is possible to know d from the end of the fiber. Then, if a certain phenomenon is modifying the grating it could be detected just by measuring the scattered wavelength. For example, if the fiber core length is modified due to a mechanical stress, or a thermal expansion or contraction, the distance d will vary, and this variation will be evident by a change in the wavelength of the scattered signal.

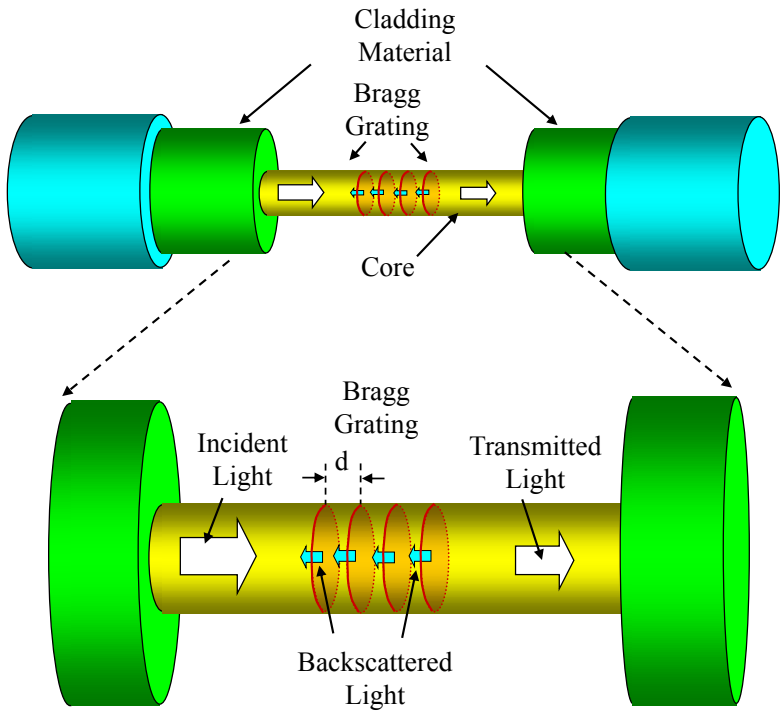

Fig. 8.2: A Bragg grating is "impressed" on the fiber core by deliberately increasing the refractive index along its length. Light of a particular wavelength is backscattered by the grating.

Thus, by means of a calibration process, the function (f) that relates temperature to wavelength may be established (Eq. (8.2)). Then we could know the temperature in as many points of the fiber as **different gratings** we could "impress" on the fiber. Usually, the process of impressing the gratings is called etching.

$$T = f(d) = f(\lambda) \tag{8.2}$$

This means that we could lay a fiber of several kilometers in length along a river or a beach to simultaneously know the temperature at many points by measuring and recording just at one end of the fiber. This constitutes a huge advantage over the process of reading and recording each one of the points individually. Many gratings can be distributed along a fiber; distances between gratings may be very close (less than 1 mm) or very far (more than 10 km). The distance from the end of the fiber to the grating is known because it is defined during the manufacturing process. The distance to the spatial point where the scattered light comes from is thus known, and so is the place where temperature is measured.

Therefore, by etching each grating with different distances d suited for specific ranges of propagating wavelengths, and placing them in well defined points on the fiber, the temperature of each specific point can be identified by the range of the scattered frequency. Thus, it is possible to know the places the scatter comes from, obtaining a graph of the temperature (by means of Eq. (8.2)) as a function of length. Hence, the temperature as a function of time and distance can be known.

When temperature at many points along the f.o. is needed, some practical limitations appear. The process of etching the grids is technologically difficult, resulting in an expensive method. But following the same ideas based on the scattering of light in f.o. we will discuss other methods that do no require modifying the fiber, as the etching of grating does.

8.1.4 Scattering in F.O.

Some conceptual insight into the scattering processes in f.o. is required to understand how some methods measure temperature by means other than gratings.

Scattering of photons inside f.o. can be produced by local changes in the characteristics of light transmission. The analysis of how the transmitted light is affected by these fiber modifications permits the f.o. to be employed as a sensor.

What it is not apparent are the internal physical processes by which the light interacts with the f.o. material producing the light scattering. Therefore to describe how f.o. work as sensors we need to introduce this subject first.

There are different types of scattering processes present in f.o., some of them known as Rayleigh, Brillouin and Raman scattering. Taking into account the energy and frequency involved in the scattering processes, two types of scattering are recognized: elastic and inelastic. In elastic scattering the scattered photons have the

same energy and frequency as the incident photons; Rayleigh scattering is elastic and is due to the fluctuations in density of the matter that produces the scatters. This kind of scattering is related to the way the molecules are organized in the f.o. material and is not of interest in the use of f.o. as a measuring device.

Conversely, in inelastic scattering, photons lose or gain energy and undergo a frequency change. A loss of energy corresponds to a down shift in frequency, and an increase in energy, to an up shift in frequency; the first is called Stokes-type scattering and the second anti-Stokes scattering.

Raman and Brillouin are inelastic scatterings and are of interest in measuring temperature and other parameters by means of f.o. Therefore, we will try a simple description of both scatterings just to gain some insight into the measuring process.

The scattering of an X-ray beam was explained in Section (3.5.1), and this explanation is valid for electromagnetic and acoustic waves. The explanation of the scattering processes in f.o. materials has two possible approaches, the classical and the quantum physics ones.

8.1.4.1 Brillouin Scattering

Electromagnetic forces due to the passage of intense laser light through f.o. produce molecular thermal agitation that sets off density changes in the fiber. These density changes propagate as acoustic waves or phonons (Selker et al., 2006). The change in density produces a change in the light refractive index that travels as an acoustic wave in the fiber. As a result, the light scattered by these moving inhomogeneities will experience a Doppler shift, and this shift can be measured from one of the ends of the f.o. as is done in the case of the method using Bragg gratings.

Because the velocity of the acoustic wave in the f.o. depends on the temperature and strain of the medium, a system devoted to the analysis of the Brillouin scattering in f.o. results in an adequate tool to perform strain and temperature measurements. From a quantum physics point of view, thermal motions of atoms in a material such as f.o. create acoustic vibrations, which lead to density variations that can be treated as a density wave or vibrational quanta (phonon). Thus, Brillouin scattering can be studied as an interaction between an electromagnetic wave and a density wave (photon-phonon scattering).

It has been found that Doppler frequency shifts of the electromagnetic wave in f.o. are linearly related to the temperature of the f.o. (Eq. (8.3)) (Minardo, 2003). Thus the f.o. becomes a temperature sensor.

$$\Delta f = K\,\Delta T \tag{8.3}$$

Summarizing and simplifying, the Brillouin scattering in f.o. is due to variations of the refractive index which travel as sound waves and scatter the light wave producing a Doppler shift on it. The velocity of the acoustic waves in the f.o. is a function of temperature so changes in temperature produce changes in the frequency shift of the scattered light. Relating frequency shift and temperature, the second may be inferred from the first.

8.1.4.2 Raman Scattering

The Raman scattering in f.o. may be thought of as the redirection of energy when the propagating light wave finds an obstacle or inhomogeneity in the material (Hahn, 2007).

Individual atoms and molecules constituting the f.o. material have specific vibrational and rotational modes (or levels) with their own vibrational and rotational frequencies (ν_{vib} and ν_{rot}).

Light is an electromagnetic wave and its associated electric field perturbs the electrons in the molecules of the f.o. material with the same frequency of the light source that illuminates the fiber (ν_s). Most of the scattered light is of this frequency (ν_s) Nevertheless, a small amount of energy is scattered at different (lower and upper) frequencies due to some complex interactions at the atomic and molecular levels between the electromagnetic wave and the material structure. The difference (or shift) in the scattered frequency is related to the vibrational and rotational frequencies of the molecular structure. As the spacing between rotational levels is small, many molecules can be excited to higher rotational levels by the incoming light. Therefore, changes in rotational modes produce dim spectral lines on both sides of the line corresponding to the exciting light (ν_s). Vibrational levels, on the other hand, are generally so widely spaced that only a few molecules are in higher vibrational levels at ordinary temperatures, and are capable of contributing with additional energy to a scattering process. Consequently, according to **Stokes law** of fluorescence, Raman lines due to changes in vibrational states are generally located towards frequencies lower than that of the exciting light (ν_s), i.e., towards longer wavelengths (called *Stokes* lines). However, dim lines are also observed towards the region of higher frequencies with respect to that of the exciting light (ν_s), i.e., towards shorter wavelengths. Since these lines have a frequency higher (shorter wavelength) than that of the exciting light (ν_s), they represent a violation of Stokes law, and are thus called *anti-Stokes* lines (Jenkins & White, 1957).

The intensities of both Stokes $P_S(z, t)$ and anti-Stokes, $P_{aS}(z, t)$ Raman scattering are functions of the light intensity, but the anti-Stokes scattering is also very sensitive to temperature. Then the ratio $R(z, t)$ (Eq. (8.4)) is independent of the intensity and depends exponentially on the fiber temperature. Therefore, measuring $R(z, t)$ allows the temperature $T(z, t)$ to be calculated (Eq. (8.4)),

$$R(z,t) = \frac{P_S(z,t)}{P_{aS}(z,t)}$$
$$T(z,t) = \frac{\gamma}{C - \ln(R(z,t)) + \Delta\alpha\, z} \tag{8.4}$$

where γ, Δα and C are calibration constants, and z distance along the f.o. (Suarez et al., 2011).

The accuracy of the temperature measurements depends on the total number of scattered photons observed; this amount increases with the time and spatial integrations of the measurements, and the proximity of the measured point to the light source (Selker et al., 2006).

8.1.5 DTS Technology in Environmental Sciences and Hydraulics

The Doppler shift of the scattered light for silica optical fibers is about 13 THz in Raman scattering, and on the order of some GHz in Brillouin scattering (Minardo, 2003). The energy associated with lattice vibrations (Raman scattering) is much greater than acoustic wave energy generated in spontaneous Brillouin scattering. In spite of these differences, both kinds of scatters have been used for DTS in hydraulics applications, but is seems that some instrument manufacturers prefer the Raman scattering for their equipment (Bao et al., 1993; Selker et al., 2006).

A simplified schematic of DTS equipment which uses Raman scattering is depicted in Figure 8.3. It consists of a laser source to excite the f.o., a detector to convert light into an electrical signal and demodulate the frequency shift, and a computer. Stokes and anti-Stokes intensity components of the scattered signal are separated and used in the computer to calculate temperature.

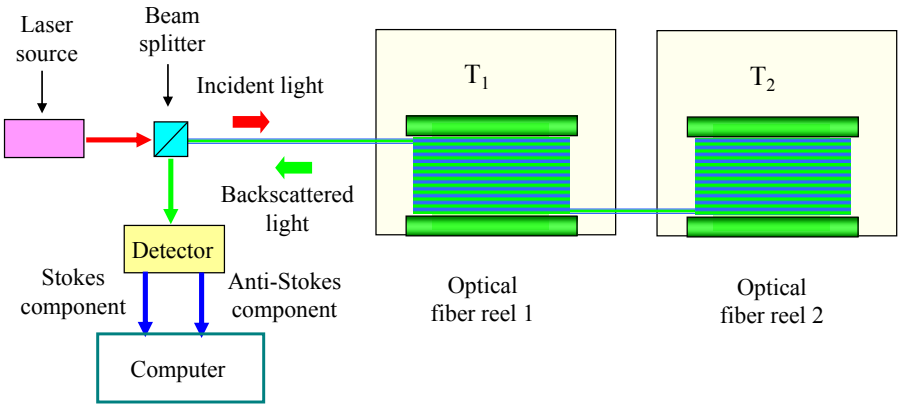

Fig. 8.3: Simplified DTS equipment measuring on an optical fiber coiled on two separate reels which are at different temperatures T_1 and T_2.

It has been mentioned that in the fiber sensors with Bragg gratings it is possible to know the distance the scatter comes from because the length from the grating to the end of the f.o. is fixed during the manufacturing process, and each grating is identified by the range of wavelengths that it can scatter. In other words, each grating

is associated with a wavelength range which in turn is related to a position on the f.o. Unfortunately, this method cannot be used with f.o. using Raman and Brillouin scatterings.

With the aim of associating the scatter with the distance it comes from in DTS it is required to send light pulses and measure the pulse round-trip travel time. This method is also known as optical time domain reflectometry (OTDR) and allows distances to be estimated; in particular, it is used in DTS to relate temperatures as a function of position along the optical fiber.

As in acoustics Doppler Current Profilers (Section (5.4.4)) and other methods where pulses are launched to obtain information about the characteristics of the medium where the wave propagates, the length of the pulse also defines the sampling resolution in space for DTS. Resolution increases as the length of the optical pulse decreases. As in the acoustic profilers, the measuring range in the fiber could be thought of as divided into a number of measuring cells over which the scatters are spatially integrated. As will be shown later, this concept is also used in radars.

Stokes and anti-Stokes scattering have different extinction coefficients, so connectors, cables, and splices have a priori unknown effects on Stokes and anti-Stokes backscatter (van de Giesen et al., 2012). For this reason, DTS techniques require carrying out an individual calibration of the instrument together with the fiber sensor (Selker et al., 2006). Manufacturers provide calibration routines that require placing sections of the cable in known-temperature baths to establish the constants of Eq. (8.4) that will be thereafter used in the measuring process.

In Figure 8.3 the fiber sensor is coiled on two separate reels that are at different temperatures T_1 and T_2. This set up is frequently used to calibrate DTS instruments and permits the spatial resolution of the ensemble to be evaluated (equipment and f.o. sensor) (http://www.sumitomoelectricusa.com; van de Giesen et al., 2012).

Some calibration algorithms assume that the f.o. parameters remain uniform over the entire length of the fiber, but more sophisticated calibration techniques and specifically designed algorithms for hydrological applications have been developed (Hausner et al., 2011; van de Giesen et al., 2012; Suarez et al., 2011). Unfortunately, temperature controlled conditions are not readily available in the field, so that field calibration is difficult.

8.1.6 Specifying a DTS Equipment

A typical way for specifying the measuring performance of DTS instruments is, for example: “a measurement with 1 m spatial resolution taken 1000 m from the instrument and integrated for 1 min will have a standard deviation on the order of 0.1 °C” (Selker et al., 2006).

As interesting as the specification in itself, which will surely change with technological evolution, is the way the instrument should be specified. These three

parameters **(distance, spatial resolution and time resolution)** define the condition in which the measuring standard deviation was established. These parameters are strongly dependent one another so that the specification makes no sense if one of them is missing. Table 8.1 shows the specifications for commercial DTS equipment (http://www.sumitomoelectricusa.com). This is not equipment easily operated in the field, but some portable equipment is emerging.

Table 8.1: DTS specifications of commercial equipment

Measurable range (km)		**15**	
Minimum measuring time (s)		40	500
Temperature resolution in °C as a function of distance	1 km	± 0.5	± 0.2
	2 km	± 0.5	± 0.2
	3 km	± 0.7	± 0.2
	5 km	± 0.7	± 0.3
	10 km	± 1.5	± 0.5
	15 km	± 3.5	± 1.0
Sampling resolution (m)	1		
Spatial resolution (m)	2		

Manufacturers' specifications for DTS equipment are **based on particular recommended fiber-optic sensor**. Then if it is attempted to make measurements on a telecommunication infrastructure already installed, as was the case of seasonal temperature profiles along the bed of a lake (Selker et al., 2006), an in situ calibration has to be performed, and perhaps the performance of the instrument could be somewhat degraded.

The utilization of DTS systems in environmental application sciences has been reported in several scientific works in recent years. They were used to observe temperature distribution along a stream, air-snow interface temperature profile, air-water interface temperature in lakes, temperature profile with depth in a flooded decommissioned mine (Selker et al., 2006), groundwater-surface water studies, soil water content interactions, tidal estuary behavior (Hausner et al., 2011), storm water sewers inspection, dam surveillance (van de Giesen et al., 2012), etc. This technology seems to have a promising future in some long spatial scale field applications in environmental sciences.

8.2 Radar

The most well known active remote sensing system is the radar; the word radar is an acronym for **Radio Detecting and Ranging**. Many remote sensing systems used in environmental sciences are based on the working principle of the early radar used to detect flying objects. Because the concepts needed to understand the first systems are easier to explain the radar, an introduction to the early radar will initially be carried out. A traditional way in which radar operating principles are introduced is by means of an acoustic analogy that we will also follow here.

If a person shouts in a big empty room, after a certain delay, a reflection of the sound on the walls will arrive back to the person as an echo. This delay is the time required for the sound to travel from the speaker to the reflecting wall and back to the speaker. Measuring the delay and knowing the speed of sound, the distance to the wall may be estimated by the product of both quantities divided by two. The divisor takes into account that the sound must travel the distance twice, to go to the reflecting object and to return from it.

A similar phenomenon occurs with electromagnetic waves. Radar emits electromagnetic energy pulses that travel through space at a constant speed of about 300,000 km/s. If the electromagnetic wave finds an object that reflects or scatters it, part of the energy will be received back at the place of the original emission. This returned signal is called backscatter or echo as in the acoustic case. As before, the product of the propagation speed of the electromagnetic wave (c) by the time delay (t_{delay}) may be employed to estimate the range (R) from the emitter to the target:

$$R = \frac{c\, t_{delay}}{2} \tag{8.5}$$

A more detailed step-by-step description of a radar signal generation and reception follows as an example.

In radar for airport traffic control, the emitting and receiving antenna is located at the center of a dish that rotates at a rate of about one turn every ten seconds (Fig. 8.4).

The dish is located at the upper end of a tower. The radar transmits short duration high-power electromagnetic pulses that are radiated into space by the transmitting antenna; when this energy arrives at the targets they produce a diffuse reflection in a wide number of directions (scatters). Some of this energy is received back by the radar antenna and the flying time of the pulse in both directions is computed. This time is used to calculate the range (distance) where the scatter comes from.

The radar's antenna is designed to radiate and detect energy in one-directional beams. They have a characteristic beamwidth similar to that described in Section (2.3.2). Thus, during the dish rotation, when the antenna illuminates the target, the direction where the reflection comes from is well known and the direction of the target is recognized.

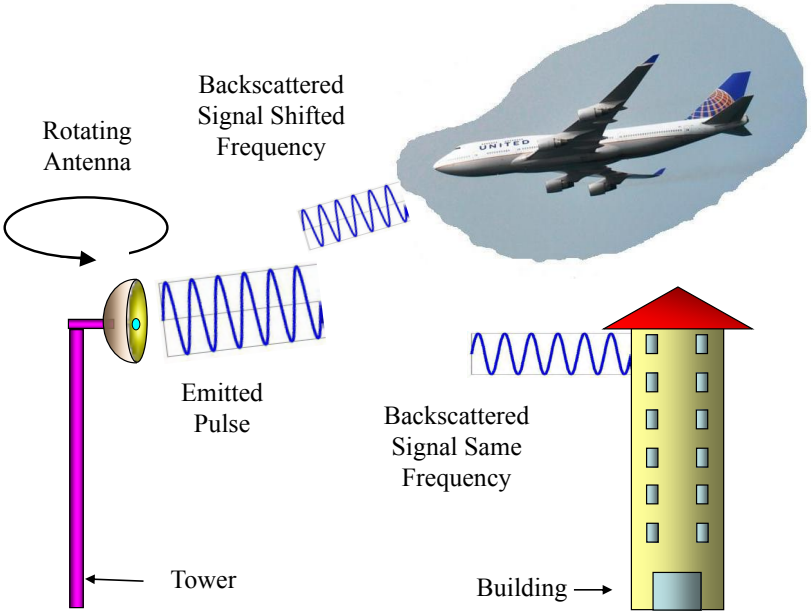

Fig. 8.4: The radar antenna rotates at the top of a tower. Fixed targets reflect the same emitted frequency. Moving targets reflect a frequency shifted with respect to the emitted one.

When the weak backscattered signals from the target arrive at the receiving antenna they are amplified and processed into the receiver. The receiver provides video output signals that can be displayed on the traditional plan position indicator (PPI) (Fig. 8.5). It consists of a circular display with concentric circles and with the rotating antenna represented at its center. Numbers on the circles are references that indicate the radial distances from the antenna measured in kilometers or miles.

As the radar antenna rotates, a radial trace sweeps the PPI display at a constant angular speed ω, synchronously with the antenna's beam. Thus, the trace indicates the pointing direction of the antenna's beam at each instant. When a target reflection is detected by the receiver a bright dot is drawn on the screen. The distance from the center of the screen to the dot represents the distance (d) from the radar to the target, thus the range and direction of the targets are shown; the PPI shows a picture of the targets present on the area covered by the radar beam.

If the target is fixed in space, as it could be the case of a building or a tree, the reflected frequency will be equal to the emitted one. But if the target is moving, there is a shift (Δf) of the backscattered frequency with respect to the emitted frequency (f_0) due to the Doppler effect (Section (3.3.1)). This shift is proportional to the product of the radial speed of the target (v) times the emitted frequency, and inversely proportional to the electromagnetic wave propagation speed (Eq. (8.6)). Therefore, the velocity of the target can also be known.

$$\Delta f = \frac{2\,v\,f_0}{c} \tag{8.6}$$

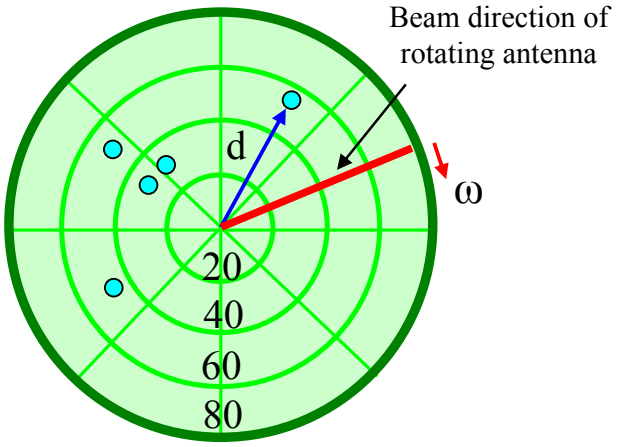

Fig. 8.5: A PPI display: the antenna beam direction is shown by the radial bar which rotates in synchronism with the antenna. Dots represent target positions. Numbers on the circles indicate their radial distances from the antenna.

A device called *duplexer* alternately switches the antenna between the transmitter and receiver, preventing the transmitted pulses from entering the receiver because their high energy could destroy the receiver. The duplexer requires a certain time to switch that is called the recovery time of the duplexer (t_{recovery}). Then those echo pulses coming from very close targets, which fall inside the transmitting pulse time (τ) plus the recovery time of the duplexer will not enter the receiver. This time in which the receiver cannot "see" the echo gives as a result a blind distance or minimum detectable range (R_{min}),

$$R_{\text{min}} = \frac{\left(\tau + t_{\text{recovery}}\right)c}{2} \tag{8.7}$$

For a typical transmitting pulse width of 1 μs (neglecting the recovery time that is characteristic of each particular radar), the corresponding minimum range is about

$$R_{\text{min}} = \frac{10^{-6} \times 3 \times 10^{8}}{2}\ \frac{\text{ms}}{\text{s}} = 150\ \text{m}$$

this means that this radar cannot detect targets that are closer than this distance.

Another important characteristic of radars is the range resolution. This is the ability of a radar system to distinguish between two targets at different ranges along the same direction. Figure 8.6 shows an example.

Neglecting radar and target particular characteristics, the range resolution depends basically on the width of the transmitted pulse (τ) and can be calculated from

$$R_{\text{resolution}} = \frac{\tau c}{2} \tag{8.8}$$

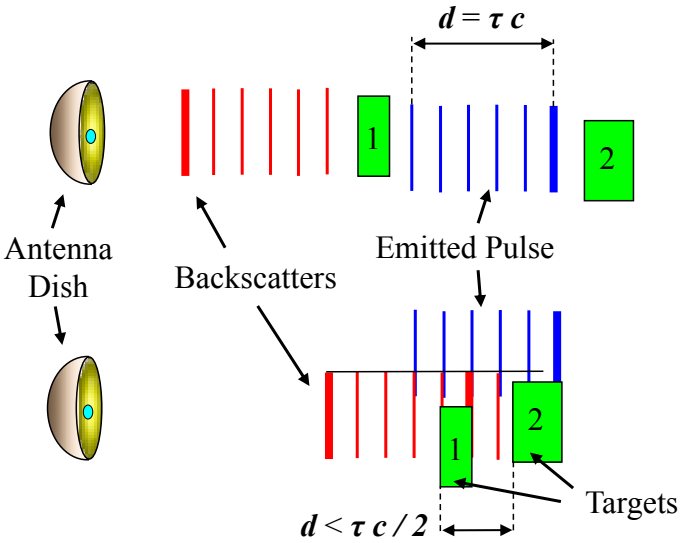

Fig. 8.6: Range resolution. The vertical parallel lines represent the radar wave fronts; the first wave front is shown thicker and a pulse is represented by six lines. In the upper part of the figure, the pulse is completely backscattered by the first target before the pulse arrives at the second target. In the lower figure the targets are closer to each other and the first target is scattering the fifth wave front while the second target is already scattering the second wave front.

The vertical parallel lines represent the radar wave fronts; the first wave front is shown thicker and a pulse is represented by six lines. In the upper part of the figure, the pulse is completely backscattered by the first target before the pulse arrives at the second target. In the lower figure the targets are closer to each other, and it shows that the instant at which the first target is scattering the fifth wave front of the pulse the second target is already scattering the second wave front. Thus, at the receiver the backscattered signals will be perceived as produced by the same object.

The range resolution and the beamwidth of the antenna define a volume that we will call the resolution cell. The shorter the pulse width τ and the narrower the beamwidth the smaller is the volume of the cell and the higher the ability to detect smaller targets (Fig. 8.7). Thus smaller cells result in higher spatial resolution.

We have mentioned that when a target is moving there is a shift of the backscattered frequency with respect to the emitted frequency due to the Doppler effect. Because the process of extracting the shift from the backscattered signal is a frequent procedure in remote sensing instrument receivers, a simple explanation of this process will be introduced.

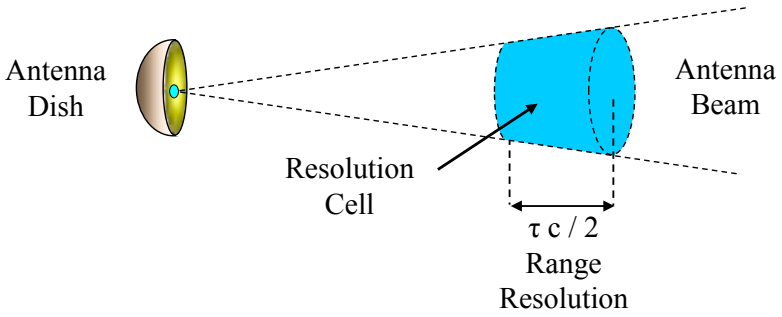

Fig. 8.7: The range resolution and the beamwidth of the antenna define a volume that we will call the resolution cell. The shorter the pulse width τ and the narrower the beamwidth the smaller is the volume of the cell and the higher the ability to detect smaller targets. Thus smaller cells result in higher spatial resolution.

Receivers used to get the frequency shift have some kind of mixer. A mixer is an analog multiplier or some kind of non-linear device that multiplies the local oscillator (LO) signal (which has the transmitter frequency) with the backscattered signal. Assuming that signals are sinusoidal, and the transmitted frequency is f_1 and the backscattered signal is $f_2 = f_1 + \Delta f$ the output $y(t)$ of the mixer is given by Eq. (8.9). As a result of the multiplying process, the difference and sum of the frequencies are obtained. Then a frequency filtering can be applied on the mixer output to keep the difference and reject the sum, thus a low-pass filtering of $y(t)$ gives a cosine signal with the frequency shift. A subsequent spectral analysis of the filter output will therefore account for the Doppler shift, and then for the velocity of the backscattering object. This kind of signal processing is called synchronous demodulation or homodyne demodulation.

$$\begin{aligned} y(t) &= \sin(2\pi f_1)\ \sin(2\pi f_2) = \frac{1}{2}\cos\left[2\pi(f_1 - f_2)\right] - \frac{1}{2}\cos\left[2\pi(f_1 + f_2)\right]; \\ y(t) &= \frac{1}{2}\cos\left[2\pi(\Delta f)\right] - \frac{1}{2}\cos\left[2\pi(2f_1 + \Delta f\right]; \\ y(t) &\Rightarrow \text{low pass filtered} \Rightarrow \hat{y}(t) = \frac{1}{2}\cos\left[2\pi(\Delta f)\right] \end{aligned} \tag{8.9}$$

So far we have used a well known type of radar to introduce some concepts. From now on we will use these concepts to describe how radar technology is applied to remotely estimate some parameters of interest in environmental sciences.

8.3 Upper-Air Remote Monitoring

One of the applications of remote sensing techniques in environmental sciences is the monitoring of upper-air meteorological parameters. Traditionally, the monitoring was done from fixed or moving instruments. Fixed instruments on meteorological towers

measured parameters such as wind velocity, atmospheric pressure, temperature, solar irradiation, and humidity. Moving instruments allow measuring some meteorological parameters as a function of altitude; radiosondes with instruments on board a flying balloon measure and transmit the meteorological data to an earth-based station. In both cases it could be said that **measurements are made "in situ"** because instruments are in direct contact with the atmosphere. One important difference is that in the balloon case the wind is inferred from its trajectory as a function of time, and it is not a direct measurement made with a fixed anemometer as in the tower case. In the first case, it is said that it is a Lagrangian measurement of the wind because a particular parcel of air drives the balloon as it moves through the atmosphere as a function of time. In the second case it is an Eulerian measurement where wind velocity is measured on a specific volume in the atmosphere through which the wind flows as time passes.

In contrast with direct measurements, ground-based remote sensing systems provide means for the collection of upper-air meteorological data, **but no instrument is in contact with the measurand**. Unlike the case of in situ measurements the remote methods are based on **indirect measurements**; this means that the desired variables are derived from other variables that are measured directly. Active remote sensing systems for measuring atmospheric data are based on sound and electromagnetic wave propagation and on how the properties of the atmosphere modify the conditions for the propagation of waves.

This difference between direct and indirect methods has significant implications for the calibration and audit of upper-air measurement systems (US EPA, 2000), because a calibration of instruments (Section (2.2.3)) in the traditional way in which their measurements are compared to those of a standard instrument cannot be performed.

The best-known systems for remote sensing of the atmosphere are: Sound Detection and Ranging (SODAR), Radar Wind Profiler (RWP), Radio Acoustic Sounding System (RASS) and Light Detection and Ranging (LIDAR).

8.4 Wind Profilers

A wind profiler is a system capable of measuring the components of wind velocity in the atmosphere as a function of altitude. This is carried out by sending a sound or an electromagnetic wave towards the atmosphere. Part of the energy is scattered by the atmosphere, received back at the point of emission and analyzed by the system. Fluctuations in the refractive index of the atmosphere, produced by air density variations, are the cause of the wave energy scatters. Because wind carries these irregularities with a certain mean velocity, these turbulences become a tracer of the wind velocity. In other words, these turbulences behave as a moving target in the case of the previously described radar (Section (8.2)).

The backscatter signals are Doppler shifted due to the wind velocity, the shift being proportional to the average wind velocity in the direction of the propagating wave. Thus, the measurement of the Doppler shifts allows the mean wind velocity to be estimated. There are different technologies based on this operating principle. Some use sound waves and others electromagnetic waves to gather wind data; a third type uses both kind of waves and it is also able to estimate the atmospheric temperature profile.

8.5 SODAR

8.5.1 General Description

SODAR is an abbreviation for Sound Detection and Ranging; they are instruments used to measure upper-air wind in the atmosphere. They consist of acoustic transmitters and receivers located at the ground level and pointing to the sky. The transmitters send pulses towards the atmosphere, and the receivers "listen" to the signal coming back from it. When the same acoustic transducer is used for transmitting and receiving it is said that the emitter and the receiver are co-located, and the system is called mono-static; when they are separated the system is called bi-static.

The earth's boundary layer has inhomogeneities called **eddies** (Bahl et al., 2011), and these eddies are transported by the wind. When the instrument emits a short acoustic pulse upward, the wave traveling through the atmosphere finds these eddies and the acoustic energy is scattered in all directions. Because eddies move at the velocity imposed by the wind, the frequency of the scattered acoustic waves is different from the frequency of the emitted pulse due to the Doppler effect. The shift of the received signal is related to the radial wind speed (speed in the direction of the propagating wave). Therefore, by measuring the frequency shifts the radial wind speed may be estimated. With this information and the geometry of the transmitter and receiver beams, the horizontal and vertical wind speed components may be calculated (Section (5.4.4)).

The height where the scattering inhomogeneities are located may be calculated from the speed of sound and the delay in the returned signal with respect to the time the pulse was sent. Thus, a profile of the wind speed as a function of height can be obtained. The transducer beam length is discretized into equal length cells as explained in Section (5.4.4) and previously in this chapter (Section (8.2)). The minimum cell length gives the maximum vertical resolution of the system.

Most of the commercially available SODAR systems are of the mono-static type and are multi-axes systems; this means that they can send and receive signals along several directions. The ability to process signals from several radial directions permits the directional profile of wind speed to be derived (http://www.sodar.com).

Because SODAR transducers are pointing up, they require weatherproof housing. Early designs used specially arranged speakers to keep precipitation out; more recently arrays of several piezoelectric transducers have been successfully used to replace speakers. These arrays have the advantage of increasing the acoustic power simply by adding more elements (Section (4.13.4)). Nevertheless, the most remarkable advantage is the possibility of using the phased-array technology. This consists in combining the individual wave fronts of transducers to give a resulting wave front for the complete array (Section (3.5.3)).

The way in which the individual transducer's lobes are combined may steer the resulting sound beam (Fig. 8.8). The electronic circuits delay the phase of each transducer in such a way that the main lobe of the array may point at some desired angle. In this way the array works as a single transducer that can sequentially gather data along multiple axes. Thus, a single array can sweep the atmosphere to obtain data from multiple directions.

The hexagon of Figure 8.8 has 19 circles and represents the acoustic transducer array, each circle being one transducer. The wave fronts represent the acoustic beam sweep. It is worth noting that the array produces one wave front at a time (even when three wave fronts are drawn they are not produced simultaneously, but sequentially).

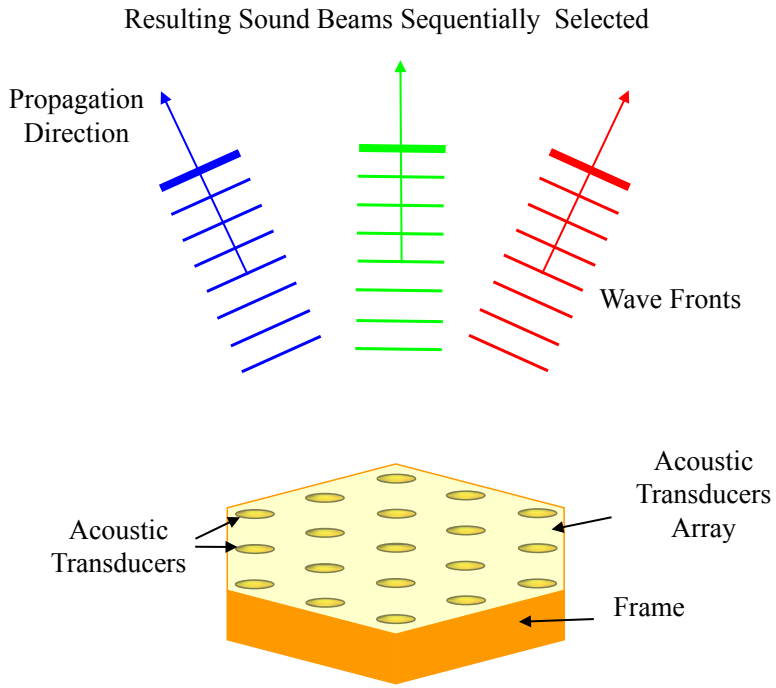

Fig. 8.8: Resulting sound beams selected one at a time.

Usually a multi-axes system consists of three to five beams. The array with five beams has a similar distribution to that shown in Figure 5.17 (Section (5.4.4.2)), in which one beam points vertically and the other four are tilted from the vertical, typically from 20 to 30 degrees. Once again, the beams are produced sequentially combining the individual lobes of each transducer by means of the beamforming process (Section (3.5.3)). Also, in the three-beam configurations, tilted lobes are placed along orthogonal directions on the horizontal plane (Fig. 8.9) (Bahl et al., 2011).

Other beam arrays use three titled beams horizontally offset by 120° (Bahl et al., 2011; Gustafsson, 2008). The beamwidth angle reported in modern literature is about 10 to 15°. The three emitting-receiving directions are switched to measure with one beam at a time (they cannot measure simultaneously in the three directions).

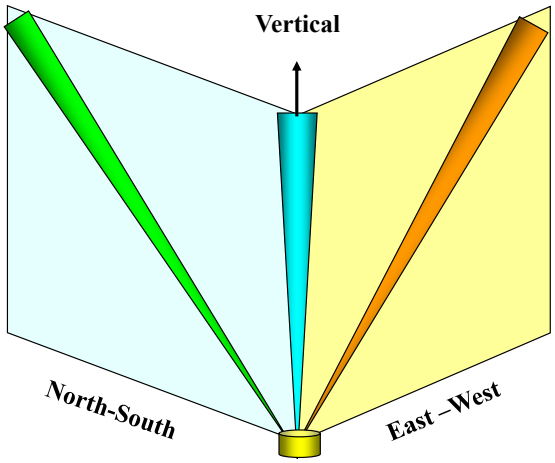

Fig. 8.9: Schematic of a three-beam configuration SODAR.

Generally, SODAR systems use the Fast Fourier Transform (FFT) to derive the signal Doppler shift. Signal averaging is used to improve signal detection, and can be performed either in the time domain or in the frequency domain (Bahl et al., 2011; Gustafsson, 2008). Due to the signal averaging, several minutes are needed to obtain a single piece of data.

It has been shown in Section (3.3.1) that the Doppler shift $\Delta f = f - f_0$ between the sent (f_0) and backscattered (f) frequencies is directly proportional to the velocity component of the inhomogeneities (v) along the wave propagation direction, and inversely proportional to the wave propagation velocity (c),

$$\Delta f \approx \frac{2\, v\, f_0}{c} \tag{8.10}$$

Because c varies with temperature (Eq. (8.11)) (Gustafsson, 2008) the actual temperature (T) in kelvins (K) is needed to correct the speed of sound,

$$c = \sqrt{401.8 \times T} \text{ m/s} \tag{8.11}$$

Before choosing a site for the installation of a SODAR system it is important to estimate the acoustic background noise level because noise may limit the maximum measuring height. Acoustic noise within the specific frequency band transmitted by the SODAR can seriously affect signal detection. Since the received signal power is inversely proportional to the square of the height it comes from, signals from greater heights are weaker and more prone to be affected by the background noise.

Another problem with a SODAR installation is that the beamwidth of the transducer (Section (2.3.2)) has a main lobe that covers the region where the desired signal comes from (upwards), but has also secondary lobes. Since these undesired lobes may point at an angle of a few degrees above the horizontal plane, the energy scattered or reflected by nearby objects such as trees, smokestacks, buildings and towers may reach the receiver. Although the secondary lobes have relative low sensitivity with respect to the main lobe, due to the great strength of the signals received from nearby objects noise may exceed the desired signal causing interference and detection problems. Thus SODAR have to be installed in open areas or a careful design should eliminate secondary-lobe effects.

For a mono-static SODAR system where the sound coming back to the receiver is only that scattered in the direction of 180 degrees, the backscatter-coefficient of the sound in the atmosphere is known as C_T (Jørgensen & Antoniou, 2002). For high wind speeds, when the turbulence can be high, C_T is low, backscattering less acoustic energy. Also, on cloudy days with small heat flux and temperature fluctuations in the atmosphere, C_T is low. Then in cloudy days with high wind speeds the signal arriving to the receiver may be so small that it could not be recovered from the background noise. Also, rain may limit SODAR operation capability (Jørgensen & Antoniou, 2002).

8.5.2 Some SODAR Characteristics

SODAR systems have maximum height ranges varying from a few hundred meters up to several hundred meters. As an example, some characteristics of two different SODAR systems found in the literature are shown in Table 8.2.

It is observed from Table 8.2 that System B with the higher altitude range has a lower spatial resolution (bigger height interval).

Table 8.2: Some Characteristics of two SODAR systems

Characteristic	System A	System B
Number of beams	3	3
Antenna beamwidth (°)	12	10
Operating frequency (Hz)	3144	2150
Pulse electrical power (W)	300	160
Horizontal wind speed range (m/s)	0-50	not available
Wind accuracy (m/s)	0.1	not available
Altitude range (m)	15-150	70-770
Height interval (m)	5	35
Averaging time for each data (minutes)	10	6

8.6 Radar Wind Profiler (RWP)

8.6.1 Introduction

The RWP is a radar system used to obtain the atmosphere's wind characteristics as a function of height. Its operation principle is based on the backscattering of high frequency electromagnetic waves due to fluctuations of the refractive index in the atmosphere caused by air turbulence.

8.6.2 Operating Principle

The operating principle of the RWP is similar to that described for the radar used to detect flying objects. Important differences are that the antenna of a RWP does not rotate and that it is installed fixed on the earth surface, its beam points vertically and pulses are emitted towards the sky. Another difference is that the antenna is composed of several smaller antennas and the set is called a phased array antenna in a way similar to the SODAR's transducer array. The signals of the individual antennas are controlled in phase and relative amplitude so that the resulting beam may be directed at different angles due to the constructive and destructive interferences of the individual wave fronts (Section (3.5.3)).

The distance and velocity of turbulent structures are estimated from the electromagnetic energy backscattered by the fluctuations of the refractive index of the atmosphere. Because these structures move with the wind speed, a profile of the

average wind speed can be described. In order to gain some insight into the RWP characteristics, a brief description of a particular high frequency RWP follows.

A RWP for studying the atmosphere's boundary layer has a phased array antenna in the 915-MHz band of about 3 m in diameter and 1 m tall. The half-power beam width (Sections (2.3.2) and (2.4.4)) is 10° and five beams are sequentially switched at times $t1$ to $t5$ (Fig. 8.10) along five different directions. One of them is vertical and the other four are placed in two vertical mutually orthogonal planes, and their directions are about 15° from the zenith. Although once again the hexagon represents the antenna array and the circles represent the individual antennas, it has to be underlined that in this case they are electrical devices to produce propagating electromagnetic waves. The beamforming process produces the five sequential beams as a result.

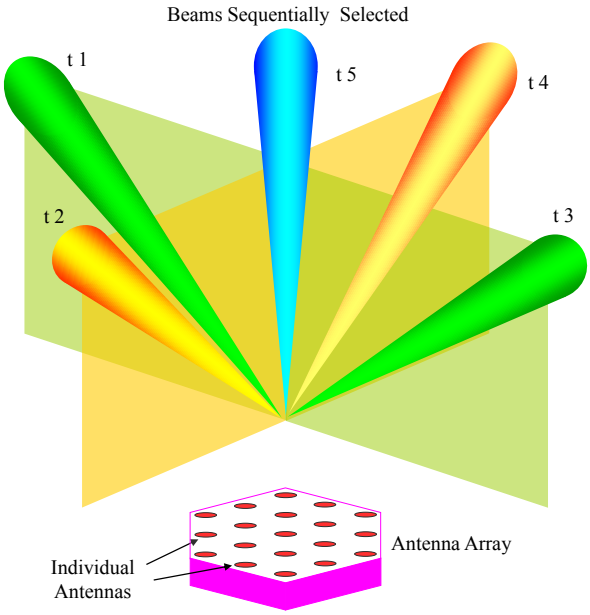

Fig. 8.10: An example of a RWP. The hexagon represents the antenna array and the circles the individual antennas. Each antenna is an electrical device which produces an electromagnetic wave. The beamforming of these individual waves produces the five sequential beams.

8.6.3 Height Coverage and Spatial Resolution

Turbulence varies with the time of the day and the height above ground level. Thus, the availability of RWP data depends on some parameters which are out of the system's user control. The maximum radar range depends on the radar frequency, transmitter

power, transmitted pulse length and antenna size, which are under the control of the designer. Sometimes the designer makes some of these parameters selectable by the users, thus making instruments more adaptable to the weather conditions.

As the height in the atmosphere increases, turbulence increases in size (DeTect, 2009), thus the upper atmosphere lacks small scale turbulent structures. As explained in Section (3.5.1) turbulent structures with sizes half the radar wavelength are needed to get the biggest backscattered energy (Bragg law). Therefore, in the upper atmosphere high frequency radar energy (small wavelengths) propagates without suffering backscattering since it does not find turbulent structures that meet the Bragg law. For this reason, lower frequency radar (longer wavelength) has to be used at high altitude to meet turbulent structures that produce strong backscattering.

There are generally three different ranges of RWP systems; the RWP for use in the boundary layer has the shortest range and transmit in ultra high frequency (UHF) around 1 GHz. Since attenuation of the electromagnetic waves usually increases with frequency they have limited height coverage of about 2 or 3 km. The frequency has to be decreased to about 400 - 500 MHz to extend the useful operation range, up to the mid-troposphere (3 to 14 km) and full troposphere (20 km).

Based on radar characteristics (operating frequency, antenna type and size, transmitter power, etc) there are mathematical models that permit the maximum reachable measuring height of RWP to be estimated. These models depend also on atmosphere's temperature and humidity. Therefore, because atmospheric conditions change with time, it is not possible to define a fixed maximum height of coverage for the RWP.

Due to the above reasons, manufacturers usually define the maximum measuring height reachable during a certain percentage of the time. According to the World Meteorological Organization (Dibbern et al., 2003), the relative availability in % is defined as

$$\text{relative availability in \%} = \frac{\text{number of valid values}}{\text{number of possible values}} \times 100 \tag{8.12}$$

Sometimes in defining the maximum measuring height reachable by a RWP it is recommended to use a relative data availability of 80% (DeTect, 2009).

There is also a minimum height below which the RWP cannot measure. It depends on the type and size of the antenna, the environmental electromagnetic noise in the installation site of the RWP, and the pulse length sent by the radar. This minimum height for boundary layer RWP is from 75 to 125 m and for tropospheric RWP, from 100 to 200 m (with availability greater than 80 %).

Similarly to the case of an Acoustic Doppler Current Profiler (Section (5.4.4)), the energy sent by the RWP antenna is a train of pulses (in the RWP, electromagnetic pulses) whose scatters contain the desired information about wind speed. Short pulses correspond to short distances along the beam direction, and then to high spatial resolution (Eq. (8.8)). As in all remote sensing systems there is a maximum

spatial resolution (minimum cell length) that depends on the transmitted pulse length. Higher frequency RWP, as those used for boundary layer, have spatial cells between 50 and 200 m. Tropospheric radar have spatial cells between 250 and 1000 m.

For the same kind of profiler (same frequency, power and antenna), longer transmitted pulses can obtain data from higher tropospheric layers because the backscattered signals are longer and contain more information, which improves the possibility of extracting the signal from the noise. But at the same time, longer pulses will produce lower spatial resolution. With the purpose of solving this compromise, some profilers can work in two modes, one using short pulses for gathering high spatial resolution data but to a limited height; and other with a longer spatial range but with lower spatial resolution.

8.6.4 Averaging Time and Accuracy

The phenomenon being measured (wind) is variable in time and space. Since the antenna beams point to different spatial regions, they may be measuring in different regions of air turbulences giving different instantaneous wind speed values. Therefore, it is necessary to time average several measurements to have representative average values; typical averaging periods are between 15 and 60 minutes.

It has been determined by long-term comparisons with radiosondes that for a one hour averaging period, wind accuracy measured by RWP is on the order of ± 1 m/s in speed and ± 3° in direction (Coulter, 2005).

8.6.5 Installation Site Characteristics

Since RWP are very sensitive to electromagnetic noise they must be installed far from highways because cars' engine sparks could produce interferences. Also, they have to be far from power lines and radio frequency transmitters. The RWP beams have to be free from obstacles such as trees, towers, and bird and aircraft flyways. Other facilities that the site should have are electrical power, availability of data communications and security. In some places an approval for radar operations may be required by local authorities.

8.6.6 How to Specify a RWP

Specifying RWP is a complex task because their performances, such as height coverage, depend on the natural variability of atmospheric conditions and the installation site environment. Some manufacturers have prepared (DeTect, 2009) technical guides to facilitate user's introduction to the subject. These guides recommend collecting as

much information as possible about the performance of commercially available wind profilers and to compare the information with users needs. As it happens with other instruments, customers sometimes require specifications that are beyond their real needs, which increase significantly the cost of the system.

8.6.7 Some Additional Considerations on SODAR and RWP Measurements

The wind data monitored by the above-mentioned measurement systems consist in volume averages rather than point measurements. Normally, radar wind profilers provide wind data averaged over 60 to 100 meter vertical intervals whereas SODAR data are typically averaged over intervals from 5 to 100 m.

The resulting data represent the average wind of the layer over which the winds are estimated. Besides their spatial averaging, data are also averaged in time. Averaging periods for wind data from SODAR and radar profilers are usually on the order of 15 to 60 minutes (US EPA, 2000).

It should be noted that systems provide measurements of mean wind speed, but variable wind information such as gusts are not available. This is because many samples in space and time are averaged to obtain one measured value.

8.7 RASS (Radio Acoustic Sounding System)

8.7.1 Introductory Explanation

This introduction presents the working principle of a Radio Acoustic Sounding System (RASS) as a general approach to the concepts involved in this measuring system. Following it, three examples with different techniques to implement the principle are described.

RASS (Radio Acoustic Sounding System) are used for remote sensing the profiles of vertical air temperature and wind speed and direction in the atmosphere (Hennemuth et al., 2012; Kartashov et al., 2008). The range of the profiles reported in the literature is variable because different electromagnetic and sound frequencies are used by different equipments; some reports mention ranges from 0.1 to 2.5 km above ground level whilst others from 1.5 up to 14 km (Chandrasekhar Sarma et al., 2008).

RASS combines the technologies developed for RWP and SODAR. Basically, it consists of an RWP array of antennas and a SODAR array of transducers emitting simultaneously upwards into the atmosphere. The operating principle behind temperature profiling is based on the effect of atmosphere temperature on the speed of sound in air; thus it results a quite indirect mean to sense the atmospheric temperature.

The principle can be explained as follows: Initially, the acoustic component of the RASS system emits an acoustic wave in the vertical direction which produces compression and rarefaction (expansion) of the atmosphere's air (Section (3.3)). These changes in the mechanical properties of the atmosphere alter the electromagnetic refractive index of the air. Note that the perturbation (sound) is a wave that travels in the atmosphere so the refractive index alteration also travels.

Simultaneously with the sound wave, electromagnetic waves are sent into the atmosphere impinging upon the altered properties of the atmosphere, producing the scattering of the electromagnetic waves. Because the perturbations are moving at the sound speed, the scattered energy will contain information on the sound speed.

The speed of the perturbations (sound) can be derived in some way from the backscattered electromagnetic signal. A profile of the speed of sound can thus be obtained, and because the sound speed changes with the atmospheric temperature the temperature profile can be inferred from the speed profile.

In order to obtain a signal easily recoverable from noise, a strong scatter is desired. There is a maximum of electromagnetic energy scattered by the altered mechanical properties of the atmosphere when the electromagnetic wavelength (λ_e) is twice the acoustic wavelength (λ_a) (Eq. (8.13)). When this condition is satisfied it is said that the electromagnetic and acoustic wavelengths are Bragg matched (Section (3.5.1)).

$$\lambda_e = 2\lambda_a \tag{8.13}$$

The propagation speed of the acoustic wave depends on the temperature and moisture of the atmosphere. By definition, the virtual temperature (T_v) expressed in kelvins (K) is $T_v = T(1 + 0.61\,r)$, where r is the mixing ratio of water vapor in the air (in kg/kg), and T the air temperature (K). The speed of sound in air (c_a) as a function of the virtual temperature is given by

$$c_a = 20.047\sqrt{T_v} \tag{8.14}$$

Because r is on the order of 10^{-3}, T_v is very close to T (T_v is at most 3 K higher than T), but with an approximate estimation of the humidity profile, corrections to get a more accurate temperature profile can be performed.

As underlined before, due to the use of the same antenna to transmit and receive, pulsed radar cannot "see" the echo during a certain time, which results in a blind distance or minimum detectable range.

8.7.2 RASS Examples

RASS theory and technology are still evolving (Hennemuth et al., 2012). Because of this, dissimilar practical configurations of the method have been implemented; all of them report good agreement between the temperature so estimated and the temperature measured by radiosondes. Some examples of this kind of systems will

follow to clarify and materialize the previously described ideas and to show some conceptual differences in the implementations of RASS.

As already mentioned, the RASS has two components, the acoustic wave generator and the electromagnetic wave generator (Fig. 8.11). It has also been explained that wind profile can be estimated by both acoustic (SODAR) and electromagnetic (RWP) waves. For the sake of clarity, some explanations are repeated below when describing the practical implementations of the following examples. Also some details are included in an attempt to visualize the different approaches for solving the same problem.

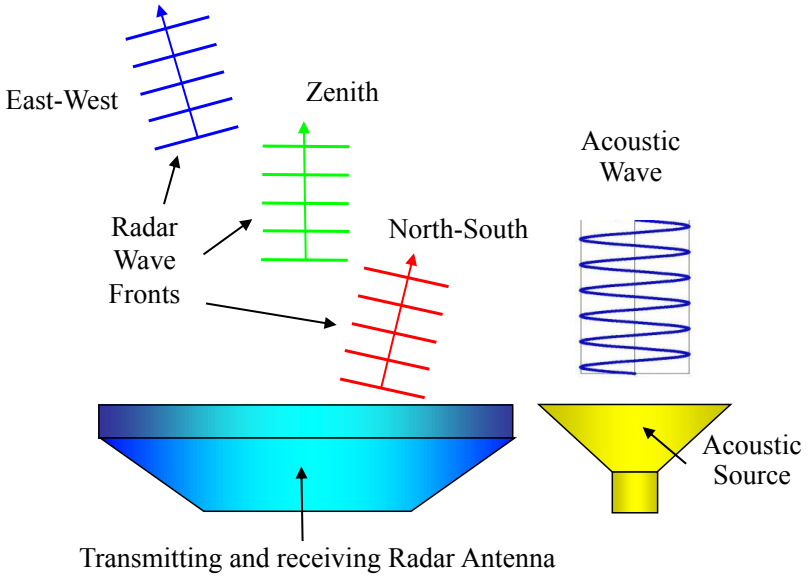

Fig. 8.11: Schematic of a RASS with its two components: the acoustic wave generator and the electromagnetic wave generator.

8.7.2.1 Example # 1

One kind of RASS is described by Pant et al. (2005); it works in a way similar to the general explanation previously described. The radar emits at 404 MHz and as in the RWP case it is capable of measuring horizontal and vertical wind velocities. The typical height coverage for wind is about 6–10 km and for temperature 2–3 km (depending on the weather conditions).

The wind profiler of the system works by emitting pulses of electromagnetic energy and switching the antenna between the emitter and the receiver by means of a duplexer (as in the RWP case). It uses an array of antennas which produce three

sequential beams, one tilted along the east-west direction, another tilted along north-south direction, and the third looking at the zenith.

As explained in Section (8.6), **the wind profile** is obtained from the fluctuations of the refractive index caused by **natural turbulence**, which produces the backscattering of the radar waves. The air with different refractive indexes is carried by the wind at its mean velocity, giving origin to a Doppler shift of the backscattered signal. By measuring this shift the mean wind velocity is inferred. A spatial resolution of 300 m for wind measurements is achieved for this particular RASS.

In a period of about one hour at least ten sets of Doppler profiles corresponding to the three beams are available. Data obtained over the total observation period are passed through a process of consensus averaging which helps to eliminate, in part, the effects of transient interfering signals, outliers, etc.

Consensus averaging consists in determining if a certain percentage of the measured values agree within a certain range of differences (e.g., 1 m/s). Those values that meet the criteria are averaged to turn out the radial wind estimate.

The temperature profiler requires combining the radar and acoustic information. The radar operates at a wavelength λ_e and the acoustic wave has wavelength λ_a. The acoustic wave propagates vertically upward in the atmosphere creating regions of compressions and rarefactions which travel at the sound speed. Thus, the acoustic wave creates moving discontinuities of the electromagnetic refractive index in the atmosphere.

When the acoustic source is operated in such a way that $\lambda_a = \lambda_e /2$ it is said that the Bragg match condition is satisfied and the electromagnetic backscattered signal increases its intensity to the maximum. The radar antenna receives strong echoes from this artificially generated diffraction grating. This backscattered signal is Doppler shifted because the acoustic wave is propagating at the speed of sound. The Doppler shift is a measure of the local sound speed at the particular height. The height (range) where the reflected energy comes from is estimated from the electromagnetic pulse round-trip travel time as in Eq. (8.5).

The speed of sound depends on the temperature at the given height where the backscattered signal comes from. Thus knowledge of the Doppler shift as a function of height permits the atmosphere virtual temperature profile to be estimated. The local sound speed is related to the virtual temperature by Eq. (8.14).

Because the speed of sound varies with height due to changes in the atmospheric temperature, for fixed acoustic and electromagnetic frequencies the Bragg match condition would be valid only at some particular heights. In order to cover all the expected sound speeds in the atmospheric region of interest, a certain range of acoustic frequencies should be generated to match the Bragg condition. For the RASS being described, whose radar wind profiler operates at 404 MHz (~ 0.74 m), the range of acoustic frequency used is between 800 and 1000 Hz to cover the Bragg match up to heights of 3 km. The authors concluded that in practice, for the temperature expected

in the place where the instrument was installed, a linear acoustic sweep interval of 40 Hz width, or a stepped approximation to such a sweep, could be used.

Going a little deeper, the Doppler shift is due not only to the speed of sound but also to the vertical component of the wind. Thus, the last must be subtracted to obtain accurate temperature measurements. If not corrected, a vertical wind speed of 0.3 m/s would result in a temperature error of about 0.5°C.

8.7.2.2 Example # 2

Another RASS system commercially available (Hennemuth et al., 2012) is quite different to the previous described. A SODAR is used as wind profiler and bi-static type radar (separated transmitting and receiving antennas) is used to measure sound speed (Fig. 8.12). Because the radar does not need to switch the antenna between transmitter and receiver, as was the case in the mono static pulsed radar, it can transmit and receive electromagnetic waves continuously. It consists of an electromagnetic transmitter at 1290 MHz and a corresponding receiver (other frequencies are also available); the transmitting and receiving antennas are separated by a distance usually between 4 and 6 m.

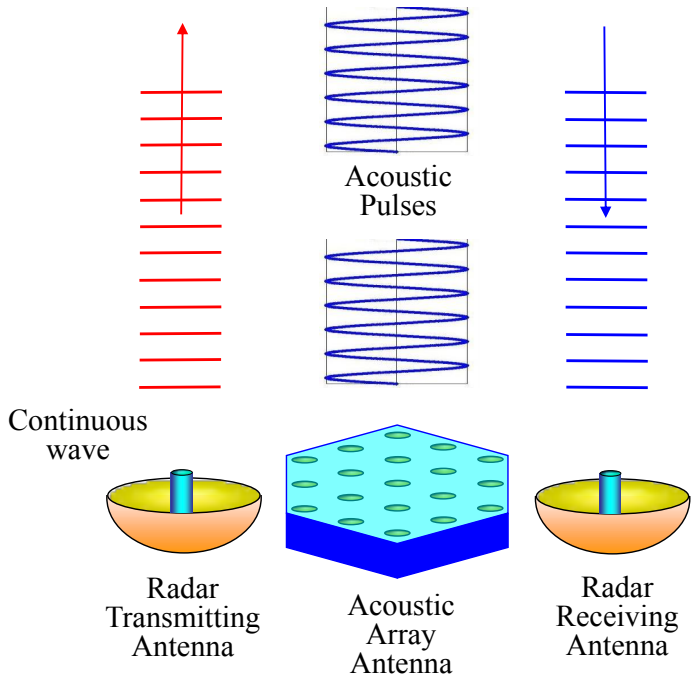

Fig. 8.12: Schematic of a RASS with an acoustic wave generator and bi-static type radar.

The SODAR component (wind profiler) of the RASS system transmits sound pulses in cycles of up to 5 beam directions and gets the Doppler shift of the acoustic signal to estimate the wind velocity (Section (8.5)). For temperature estimation the transmitting cycle of the SODAR is extended with an additional (sixth) sound pulse devoted to sound speed profiling. The Doppler shift of the electromagnetic wave due to the rarefactions produced by this extra acoustic pulse is used to estimate the speed of sound.

Two Doppler shifts are thus taken into account; one of them is the shift of the acoustic wave due to wind speed, and the other is the shift of the electromagnetic wave due to the travelling rarefaction produced by the sixth acoustic pulse. Once the acoustic and electromagnetic shifts are drawn from the respective signals, the same hardware and software can be used for processing the SODAR as well as the RASS echoes because the signal properties of both shifts are very similar (Hennemuth et al., 2012). With this system the temperature profile is known with a height resolution of 10 m, beginning at 35 m above ground level.

The use of bi-static radar permits the lower few hundred meters of the atmosphere to be sampled. It has been reported that this bi-static RASS system improves the overall quality of temperature profiles in the lowest 300 m. The disadvantage is that it requires a correction because the scattering angle is not exactly 180° and is a function of height.

8.7.2.3 Example # 3

Some characteristics of a commercial RASS system were evaluated by a US government agency (Coulter, 2005); they are summarized below. This RASS electromagnetic wave transmitting frequency is 915 MHz and its maximum range is from 3 to 5 km, depending on the atmospheric conditions. According to Coulter (2005), daily comparisons with data derived from radiosondes during more than one year gave the following quality figures:

Accuracy for wind speed: 1 m/s

Accuracy for radial wind components along the transmitter's pointing direction: 0.5 m/s

Accuracy for wind direction: 3°

Accuracy for virtual temperature: 0.5 K

This RASS uses a square antenna array of approximately 4 m side that transmits electromagnetic waves alternately along five pointing directions, one vertical, two in the north-south vertical plane and two in the east-west vertical plane. The distribution of the beams is similar to that shown in Figures 5.17 and 8.10; the beams are tilted about 14 degrees from the vertical. The system includes four fixed acoustic sources located at the corners of the antenna to estimate temperature profile (Fig. 8.13).

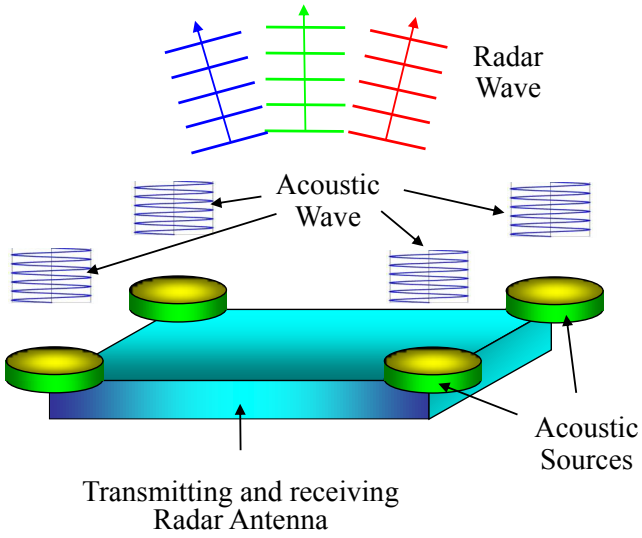

Fig. 8.13: Another type of RASS with a transmitting and receiving radar antenna and four fixed acoustic sources.

The radar transmits sequentially in each beam direction and receives backscattered energy from refractive index fluctuations that are moving with the mean wind speed. Radial components of motion along each pointing direction are determined. It takes 30 to 45 s to determine the radial components from a single pointing direction.

The system cycles through the five beams at low power, and then it cycles again at a high power (longer pulse length); the whole process is repeated every five minutes. About 12 estimates from each beam are saved for an averaging interval of one hour; these values are evaluated at the end of the period to determine the consensus-averaged radial components of motion. The radial values are then combined to produce the wind profile. The wind data reported by the system are: height, speed, direction, radial components, number of values in consensus, and signal to noise ratio.

When the beam of the radar is pointing vertically, an acoustic pulse of about 1-10 kHz is transmitted simultaneously into the atmosphere. Now changes in the index of refraction produced by the travelling sound wave are the source of the radar wave backscattering. The combination of the sound wave speed and the vertical wind velocity is estimated from the Doppler shift of the backscattered wave. Then it is sometimes necessary to compensate for vertical wind. Finally, the temperature profile is estimated from the sound speed as in the previous examples. The averaging time for this estimation is about 10 minutes. In normal operation, temperature profiles are determined during the first 10 minutes of every hour and the wind profile is averaged over the remaining 50 minutes.

8.7.3 Summary and General Considerations about RASS Systems

Wind speed in RASS systems is determined from the Doppler frequency shift of the waves, which are scattered due to **natural fluctuations in the refractive index** present in the atmosphere. The waves may be either acoustic (as in SODAR) or electromagnetic (as in RWP).

The virtual temperature is determined from changes in the speed of sound in the atmosphere. With the purpose of measuring the speed of sound a vertical sound wave is generated which **induces changes in the refractive index of the atmosphere**. The detection of the propagating velocity of this diffraction grating can be performed by means of the Doppler shift of the backscattered **electromagnetic wave.** The directly measured parameters have to be converted into the parameters of scientific interest: wind velocity and temperature profiles.

When analysing data from RASS systems, it should be taken into account that the wind speed is derived from backscattered signals coming from several beams spatially separated. To obtain the wind vector at a single height, the information of the cells of all the beams at this particular height are processed. The estimation of the wind assumes that the phenomenon is horizontally homogeneous, which could not be true. When the height increases, the separation between beams increases and the cells taken to calculate the wind are further apart.

Frequently Asked Questions

Coulter (2005) found that a very frequent question from users of RASS and balloon sounding system (or radiosonde) is: Why don't the profiler's values of winds and/or temperature agree with values from radiosondes?

This question should not surprise us because as explained in Section (7.2.4), even two anemometers installed close to each other, with the same operating principle but different rotation sensors (propeller and cup), measure different wind values; moreover, different cup anemometers (same rotation sensors) have different behaviors in turbulent wind (Section (7.2.4)).

These behaviors are due in part to differences in the transference of sensors; that is to say, both instruments respond in different ways to the same stimulus. But it is also because wind is not the same even in close proximity; in other words the stimulus changes spatially and instruments are "sensing different winds".

The answer to the frequent question follows the same reasoning as above. Actually, each instrument (RASS and radiosonde) "senses" the stimulus in a different way because they average the measurand with different time and spatial constants (different filters). The radiosonde measures with "traditional" instruments with high spatial resolution and fast time response; profilers, instead, average over greater volumes of atmosphere and average several measurements over a longer time. Also, it is true that they do not measure the "same" wind or temperature.

As introduced in Section (8.3), radiosondes perform spot measurements and travel with the mean wind in vertical and horizontal directions simultaneously; they do not measure in a vertical direction. The RASS measures over the same vertical column of the atmosphere and the resulting data is the outcome of values measured over a volume, which was previously defined as the resolution cell. This cell can range from tens to hundreds of meters in length, and have the diameter of the antenna beam. The RASS provide values averaged over a long time (usually 1 hour) and the radiosonde measure at one instant. Another difference is that the radiosonde measures the temperature directly and the RASS estimates the temperature from the speed of sound.

Summing up, the balloon sounding system and the RASS measure on different volumes of the atmosphere; that is to say, they measure different stimuli; the spatial and time scales of both measurements are quite different.

As a preliminary conclusion, it has to be accepted that understanding how instruments work allows us to recognize what is the measurand they are really measuring and why differences in measurements appear. These are some of the goals of this book.

8.8 LIDAR (Light Detection and Ranging)

In the same way as radio frequency waves are used by radar to study the atmosphere, the lidar uses laser pulses of very high frequencies (some in the frequencies of visible light) with the same purpose. Because of the small wavelengths (~ 0.4 - 2 μm) and high directivity of lasers, laser pulses are scattered by small dust particles (aerosols), particles much smaller than those "seen" by radar waves. The spatial resolution of the lidar is of a few meters, resulting much better than that of the radar. Often, the lidar wavelengths used for atmosphere studies range from the ultraviolet to the infrared.

Figure 8.14 is a schematic of the functioning principle of a lidar for the survey of atmospheric parameters. A laser is pointed vertically into the atmosphere and an optical amplifier system (such as a telescope) is pointed toward the laser beam. Aerosols, atmospheric gases and water drops, scatter the laser light along its path.

The optical signal captured by the telescope is filtered and focused on a photomultiplier that converts optical signals into electrical signals. The electrical signals, containing the information of the laser scattered energy, are digitized and processed by a computer, in a similar way as it is done in the radar system. In order to get Doppler shifts the backscattered signal is mixed with an optical local oscillator and then low-pass filtered in the same way as was explained for radars (Eq. (8.9)).

The frequency shift of the backscatters is a measure of the radial wind speed in the lidar line of sight. The distance (range) to the backscattering object is estimated from the pulse propagation speed (light speed) and the round trip flying time of the pulse.

As laser pulses propagate, they illuminate fractions of the atmosphere along the beam direction. Therefore, backscattered signals can be associated with given distances from the emitter; the time delays between pulses sent and received back permit the distance from the lidar to the analyzed zone of the atmosphere to be estimated.

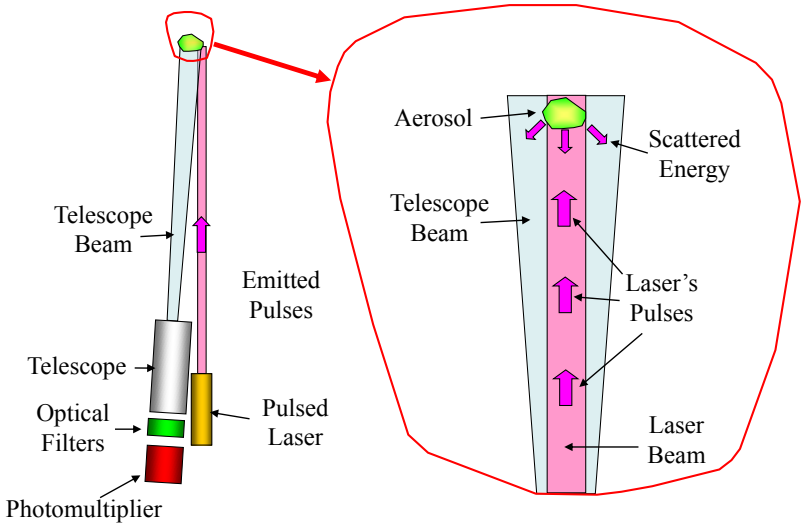

Fig. 8.14: (Left) The elements composing the lidar. (Right) How the laser signal is scattered and captured by the optical system.

Precision timing circuits segment the returned signals into a number of shorter time periods. These periods are linked to specified segments of the radial distance along the beam, called **range gates**. The concept of a range gate is similar to that described in radar systems, where it was called cell length (Section (8.2)). The backscattered signals within each range gate are used to calculate the average radial wind velocity for each gate. This process is repeated all along the beam.

The maximum lidar range depends on the pulse length, the power of the laser and the weather conditions. For example, for a commercial pulsed laser at 1.54 μm (near infrared), with a 50 m long pulse, a maximum height of 6,000 m can be reached under certain atmospheric conditions (http://www.leosphere.com). The minimum range depends also on the pulse length. The emitted laser pulse is so intense that at the first instants of the emission the fraction of the lidar pulse captured by the optics (telescope, filters, etc.) is more intense than the light backscattered by the atmosphere. Then there is a time window in which the lidar is blind, as it happens

with radars, and this blind time fix the minimum measuring range. For the same lidar as above, a 50 m long pulse results in a minimum range of 100 m.

The laser sends to the sky high energy pulses of some hundreds of nanoseconds of duration (τ). This duration defines the spatial resolution of the measuring system (S_{res}). It is the ability of a lidar system to distinguish between two targets at different ranges along the same direction (Eq. (8.15)) (as explained for the radar case in Section (8.2), Eq. (8.8)).

$$S_{res} = \frac{\tau c}{2} \tag{8.15}$$

where c is the speed of light (3×10^8 m/s). Table 8.3 presents examples on how pulse duration, length of pulse and spatial resolution are related.

Table 8.3: The relation between pulse duration and length and spatial resolution

Pulse duration (ns)	Pulse length (m)	Spatial resolution (m)
100	30	15
800	240	120

The pulse repetition rate (*prr*) should be as high as possible in order to have a more frequent scanning of the atmosphere, i.e., to have more useful information, but it cannot exceed a maximum value to avoid ambiguity between returned signals (Eq. (8.15)). The time between pulses (1/*prr*) must be longer than the round trip time of flight of the pulse to the greatest height to be measured (h_{max}) (Eq. (8.16)) (Cariou & Boquet, 2011). Table 8.4 shows examples of *prr*.

$$prr_{\max} = \frac{c}{2h_{\max}} \tag{8.16}$$

Table 8.4: Examples of pulse repetition rate (*prr*)

Maximum height reached (m)	Maximum pulse repetition rate (kHz)
15,000	10
300	500

As stated above, the lidar measures the radial component of the wind or, in other words, the projection of the wind vector on the laser beam. Thus the schematic presented in Figure 8.14 would be able to measure only the vertical component of wind. Therefore, to provide the ability to measure the wind vector along other directions the beam is headed by means of a device called scanner. It moves the

measuring array so as to direct the laser beam upwards along the lateral height of a cone around the zenithal direction (Fig. 8.15). The radial components are combined by means of simple trigonometric relations to get the wind components in the *x*, *y* and *z* directions. For these relations to be applied, some assumptions are made: (i) at a given altitude wind velocity is homogeneous in a horizontal plane; (ii) temporal variations in wind velocity are slow enough so as to consider that all measurements are simultaneously performed; and (iii) wind can be considered as constant in each one of the spatial cells into which the laser beam is divided.

The lidar beam may suffer attenuation due to three processes acting simultaneously in the atmosphere, namely energy absorption by molecules, molecular scattering and particle (aerosols) scattering. With intense fog or low clouds, the lidar cannot operate due to the high atmospheric attenuation

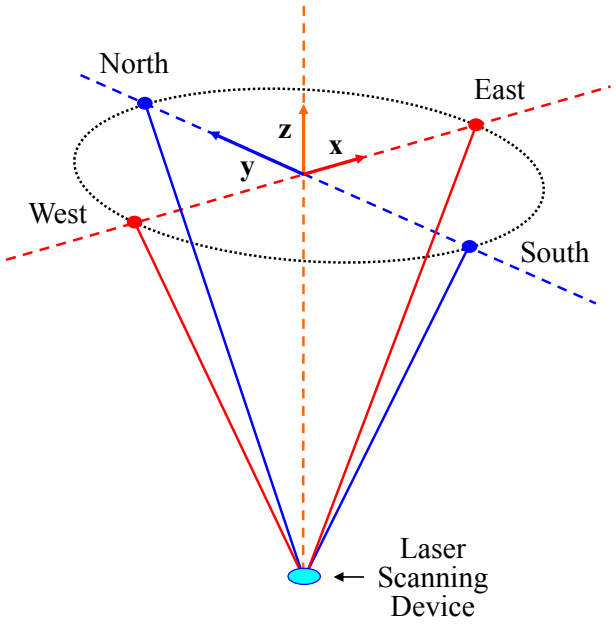

Fig. 8.15: The system shown in Figure 8.14 is rotated for the beam to describe an inverted cone with a vertical axis. The small dots represent the range gates (spatial cells) where the wind radial components are measured to be later converted into wind components along the *x*, *y* and *z* directions.

For the laser beam to be eye-safe it must be of wavelengths greater than 1.4 μm. The improvements of solid state laser technology makes the near infrared spectrum (1.4 μm - 2.2 μm) widely used for wind measuring lidar because they have good sensitivity to Doppler shift, good atmospheric transmission and are eye-safe (Cariou & Boquet, 2011; Rocadembosch et al., 2003).

Classic lidar systems emit very short high power laser pulses, but there are systems based on solid-state technology, known as microlidar, which are eye-safe and of low cost. They are of low power and modulate the optical carrier with pseudorandom sequences that permit the information from the noise to be extracted easier.

Lidar may have quite different specifications according to the desired application. For example, there some lidar used to evaluate installation sites for wind farms, which measure on a short range with great accuracy. Technical specifications of a commercial lidar for wind farm evaluations are presented in Table 8.5 (http://www.leosphere.com). Another lidar from the same reference, but for larger range applications, is presented in Table 8.6.

Table 8.5: A commercial lidar for wind farm evaluations

Range Min-Max	**40 to 200 m**
Data sampling rate	1 s
Number of measurement cells	12
Speed accuracy	0.1 m/s
Speed range	0 to 60 m/s
Direction accuracy	2°

Table 8.6: Another lidar, but for larger range applications

Maximum range	**15,000 m**
Wind measurement range on aerosol, depends on the range gate width and the accumulation time.	100 – 10,000 m 50-2,5000 m
Averaging time	1-10 s
Range gate width	20-50-100 m
Number of programmable gates	120-240
Radial wind speed accuracy	0.2 m/s below 1,500 m; 0.3 m/s above
Cloud detection	15,000 m
Azimuthal scanning	0 to 360°
Elevation angle	-10 to 190°
Angular resolution	0.5°
Maximum rotation speed	4°/s

Lidar are used to estimate the density of aerosols, the speed and direction of wind, the concentration of chemical species, temperature profiles and to measure height and thickness of clouds. When buying a lidar, it should be chosen according to the desired parameter to be studied (Rocadembosch et al., 2003). Also, lidar onboard ships and helicopters are used to measure coastal bathymetry; onboard planes, are used to get images of cultivated areas, canopy and forests. For more information on these applications more specifics books should be consulted (Campbell, 2008).

8.9 Weather Radar

The upper-air remote monitoring systems presented hitherto use fixed antennas placed at the ground level that are pointing to the sky. Instead, the weather radar is similar to the radar for airport traffic control, which has a rotating antenna for emitting and receiving electromagnetic waves (see Section (8.2)).

In order to understand the working conditions of the weather radar it is convenient to turn back briefly to the scattering of X rays by a crystal lattice (Section (3.5.1)). Recall that we had underlined that two matters were worth noting in the scattering of X rays by a crystal lattice, as well as in the scattering of electromagnetic and acoustic waves in general. First, the dimensions of the scattering sources are smaller than the wavelength of the incident wave and second, the distance between scattering centers is comparable to the incident wavelength. This is exactly what happens with weather radar systems used for detecting and quantifying rainfall. The dimensions of the scattering sources (raindrops) are smaller than the wavelength of the incident wave (on the order of some centimeters), and the distance between scattering centers (raindrops) is comparable to the incident wavelength. Therefore, because of the size of precipitation, most radar systems used to estimate rainfall are in the C-band microwave frequency, for example 5.6 GHz, which gives a wavelength of about 5 cm (Mushore, 2012). These radars have a spatial resolution of 2.5 km and provide a reflective map every 5 minutes.

The radiation backscattered to the radar antenna is proportional to the density of the water particles. In a volume of atmosphere illuminated by the radar, the power of these scatters is proportional to the sixth power of the particle diameter. Therefore, the radar reflectivity Z (or reflective factor) is (Mushore, 2012)

$$Z = \sum_i N_i D_i^6 \tag{8.17}$$

where N_i is the number of drops with a diameter D_i per unit volume of air.

The energy of the returned pulses depends on the amount of particles, particle size and shape, and particle state (solid or liquid):

(http://www.bom.gov.au/australia/radar/about/what_is_radar.shtml)

In order to scan a higher volume of the atmosphere, the elevation angle of the radar is not fixed as in the case of the traffic control radar, but the antenna is tilted

after each rotation, thus it scans a different volume of the atmosphere each time (Fig. 8.16). This procedure is automatically repeated several times until the maximum tilt angle is reached. All the procedure takes a few minutes.

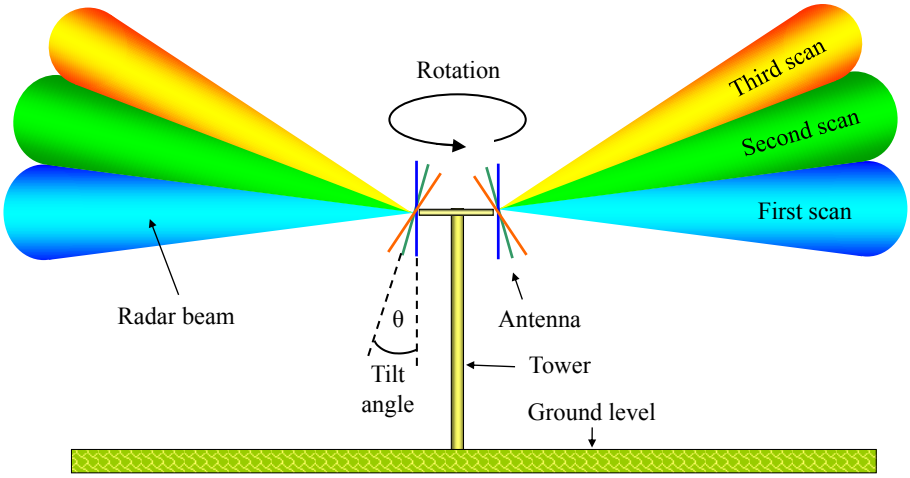

Fig. 8.16: The antenna rotates and the beam scans the atmosphere. After the first complete rotation the antenna is tilted and a second rotation begins. Each scan of the beam is shown with a different color.

The reflective factor Z (mm^6/m^3) must be converted into rain rate R (mm/h) using the reflectivity-rain rate (Z-R) relationship (Mushore, 2012):

$$Z = a\,R^b \tag{8.18}$$

where a and b are empirical coefficients. This means that a calibration has to be performed for each radar system in order to obtain such coefficients.

Rain radar data is generally presented to the users as an artificial colored map where each color corresponds to a different intensity of the precipitation. The map represents a given geographical area that depends on the radar range. The center of the map corresponds to the position of the radar. As shown in Section (8.2), this kind of map is called plan position indicator (PPI).

Due to the drag coefficient of air, falling-rain droplets are larger in the horizontal axis than in the vertical one. For this reason, in order to receive the maximum signal reflection from precipitation, traditionally C-band radar send horizontal polarized radar waves. In recent years, some radar systems are being modified to send alternatively horizontal and vertical polarized waves. This strategy allows more information about the shape and other precipitation's characteristics to be obtained. The new kind of radar is called C-band polarimetric radar or dual polarization radar.

Its operation is based on the fact that rain, solid precipitation, birds, insects, etc, produce different vertical and horizontal scatters. It is said that they have different reflective factors in both directions (Z_v and Z_h, respectively). For example, the ratio Z_v/Z_h is a good marker of the rain drop shape.

In spite of the capability of the meteorological radar to estimate precipitation in real time over large areas, measurements are affected by some sources of errors. One source of systematic errors is the reflectivity-rain rate relationship (Z-R) utilized to transform the radar reflectivity maps into precipitation maps (Piccolo & Chirico, 2005). For example, for the Royal Netherlands Meteorological Institution (KNMI) these coefficients are $a = 200$ and $b = 1.6$. But in a study performed for a particular area of the Netherlands it was found that the coefficient a ranged from 70 to 115, and the coefficient b from 1.1 to 1.7 (Mushore, 2012). Other used values for these coefficients are: $a = 300$ and $b = 1.4$ (Hunter, 2009). Therefore, adopting incorrect values for these coefficients could be an important source of error.

Improving the calibration of this relationship for a particular area can reduce these errors. This is done by correlating the radar data with a considerable amount of rain gauge data recorded simultaneously over a long period of time.

Another source of error is that if radar detects rain that does not reach the ground, then radar information does not agree with rain gauges installed at ground level. This phenomenon is called Variable Intensity Rain Gradient Aloft (VIRGA) and it happens when falling from a cloud, rain or hail evaporates before arriving at the ground (http://www.bom.gov.au/australia/radar/about/what_is_radar.shtml)

Because of the Earth's curvature and the decrease in the atmosphere refractive index (due to the decreasing density as height increases) the radar beam draws away from the Earth's surface. Thus, the beam of the radar does not detect rain in the low atmosphere when it is far from the radar. For example, radar that estimates 100 per cent of the actual rain-gauge amount at close ranges, detects only 25 per cent at a range of 100 km (World Meteorological Organization, 2008).

More recently, some errors were found to be introduced by the temporal and spatial scales that the radar utilizes in estimating the precipitation (Piccolo & Chirico, 2005). That is, the spatial resolution of the radar, the time interval between radar scans and the time performing each scan, play an important role in the results. In this research one C-band dual polarization radar with high spatial and temporal resolution was used. The range resolution was 75 m and a complete PPI could be acquired in just one minute (when a single elevation angle was used). In processing the data three different spatial scales (600 m, 1200 m and 2400 m) were used, which are close to the typical spatial resolutions of commercial operational radars.

This work showed that the error made in the estimation of the accumulated rainfall map can be significant for the sampling interval of 5-10 min usually employed in operational radars. In particular, for a 10 min sample interval with spatial scales between 600 m and 2400 m, the Normalized Standard Error ranges from 20 to 30 %, with error decreasing as the spatial scale increases.

Radars have the capability of measuring over inaccessible areas but are less suited to give accurate absolute rain-amount information. It is unlikely that radars will replace rain gauges because rain gauges provide additional information and are necessary to calibrate radar measurements. Radar is useful for the detection of potentially severe thunderstorms and tornadoes; also, digital processing of reflectivity can be used to detect hail. Nowadays computer systems can blend radar data from some radar with other type of information such as rain gauge data. The use of the Doppler effect on weather radars has led to the identification of some characteristic patterns or "signatures" of some meteorological phenomena such as a vertical column of rising rotating air (typically 2 to 10 km in diameter) called mesocyclone (World Meteorological Organization, 2008).

8.10 Measurement of Sea Surface Currents

Sea surface currents may be remotely estimated by means of high-frequency (HF) radar installed on the shore. The radar antenna emits electromagnetic pulses in the frequency range from 3 to 30 MHz, the corresponding electromagnetic wavelengths (100 to 10 m) being comparable to those of the mechanical surface ocean waves. For some wavelengths there exists a resonant backscattering of the electromagnetic wave emitted by the radar (Paduan & Rosenfeld, 1996). The scatters which arrive back to the shore are captured by means of antennas disposed in special arrays co-located with the emitting antenna The HF radar signal scattered by the sea waves contains information on the surface ocean currents.

Within the above-mentioned radar frequency band, sea waves will produce a Bragg scattering when the wavelength (λ_R) of the radar pulse is twice their wavelength (λ_S) (Section (3.5.1)). To see why this is so, consider the schematic of a HF radar (O) located at a height z over the sea shore (Fig. 8.17).

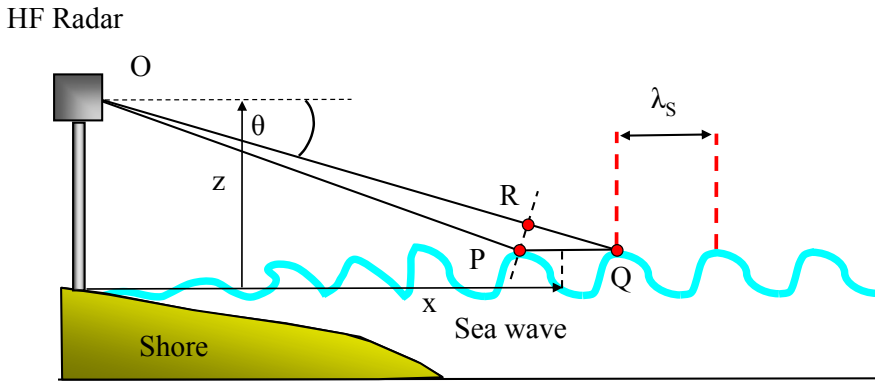

Fig. 8.17: Schematic of HF radar beams impinging sea waves.

A beam of rays strikes the crests of two consecutive waves, P and Q, located at a mean distance *x* from the shore. Let θ be the angle that the beam makes with the horizontal. The HF radar waves are backscattered by the sea wave crests P and Q and captured by the receiver antennas. A radar wave front drawn through P intersects the ray OQ at R (recall that a wave front is perpendicular to the direction of wave energy propagation). In the triangle PQR, the angle at Q is also θ.

Now, on coming back to the receiver antenna, the backscattered radar wave that struck the sea wave crest at Q will have traveled an additional distance 2 RQ = 2 PQ cos θ with respect to the radar wave that struck the sea wave crest at P. Since the angle q is very small, cos θ ≈ 1, so 2 RQ ≈ 2 PQ = 2 λ_S, where λ_S is the wavelength of the sea wave. If the backscattered radar waves are to arrive at the receiver antenna so as to interfere constructively, i.e. if they are to arrive in phase, the additional distance 2 λ_S must be an integral multiple *n* of the radar wavelength, i.e.

$$2\,\lambda_S = n\,\lambda_R \tag{8.19}$$

where λ_R is the radar wavelength. Since the maximum energy of the backscattered wave is obtained for $n = 1$, it follows from Eq. (8.19) that this is equivalent to $\lambda_S = \lambda_R/2$. This is again the Bragg matching concept already presented in Section (3.5.1). In other words, for a radar frequency band from 3 to 30 MHz, the maximum radar wave energy arriving at the receiving antenna comes from those waves that have been backscattered by sea waves with a wavelength range from 50 to 5 m.

The Bragg scattering produces a very large energy peak at the receiver whose frequency can be determined accurately among the reflections from other surfaces (Paduan & Rosenfeld, 1996). The received signal, which carries the information on the sea waves, can thus be processed.

Because the target (sea waves) is moving at a certain velocity (*v*), the backscattered frequency is shifted with respect to the frequency sent by the radar due to the Doppler effect. The shift (Δ*f*) of the backscattered frequency with respect to the radar-sent frequency (f_0) is proportional to the target velocity (*v*); they are related as in Eq. (3.8) (Doppler effect).

Two mechanisms are recognized in the wave displacement: the surface current speed (*Vsc*) and the phase speed of waves (*u*). Then Eq. (3.8) is presented slightly modified in Eq. (8.20), where *c* is the propagation speed of the electromagnetic wave.

$$v = Vsc + u = \frac{\Delta f\ c}{2 f_0} \tag{8.20}$$

According to the linear Airy water wave theory (or small-amplitude water wave theory), a sea wave of wavelength λ_S is considered to be a deep-water wave if it is in water of depth $h > \lambda_S/2$. The phase speed of deep-water gravity waves (*u*) is given by (Kinsman, 1965; Dean & Dalrymple, 1984; Sorensen, 1993) as

$$u = \sqrt{\frac{g\ \lambda_S}{2\pi}} \tag{8.21}$$

where *g* is the acceleration due to gravity. Therefore, since the emitting frequency of the radar (λ_R) is known because it is a characteristic of the radar defined when it is manufactured, and as $\lambda_S = \lambda_R /2$ due to Bragg law; *u* may be calculated from Eq. (8.21), and *Vsc* from Eq. (8.20). Thus, the surface current speed is obtained.

In order to get a reliable estimate of the spectral peak of the backscattered signal it is necessary to spatially average many observations over the sea surface and also over time. The range covered by this kind of radar is usually from 15 to 70 km, depending on the operating frequency, transmitted power and sea state conditions. Spatial resolution is about 3 km.

The calculated surface current speed is an average estimated over a depth on the order of 1 to 2 m (Paduan & Rosenfeld, 1996; Laws, 2001), depending on the radar operating frequency. High-frequency electromagnetic waves sample the sea current closer to the surface than low-frequency waves do.

The spectrum of sea echoes contains two well defined peaks shifted between about 0.2 and 0.6 Hz from the transmitted radar frequency. From these peaks surface sea currents are estimated (Laws, 2001).

The Bragg scattering occurs for waves traveling in the direction of the propagating electromagnetic wave (i.e. directly towards the radar or away from it), so in order to get a two-dimensional current map over a sea area it is necessary to measure with at least two radar (*A* and *B*) located at different places (Fig. 8.18); the information of both must be combined to estimate the vector current.

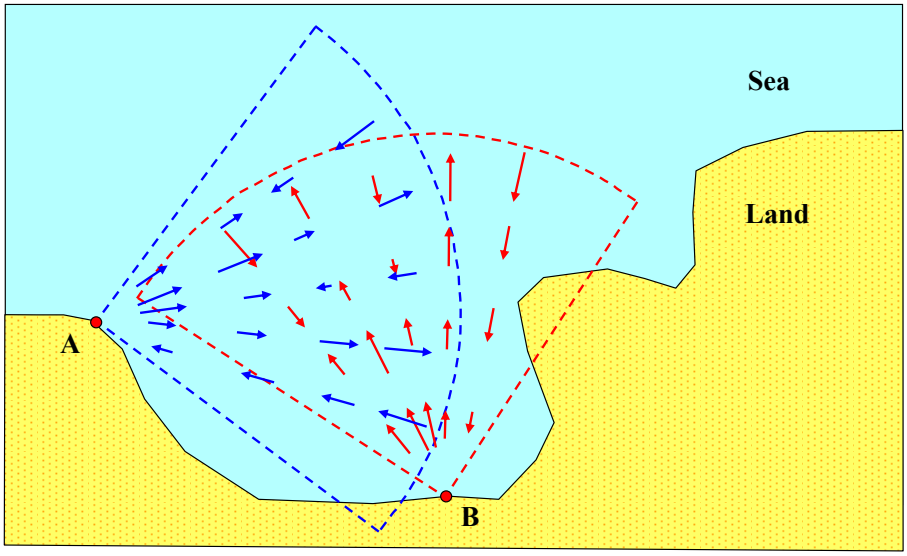

Fig. 8.18: The circles A and B indicate the shore installation of two radar (*A* and *B*). The dashed lines indicate the sea surface area covered by both radar systems. The arrows indicate currents measured by each of the radar. They must be composed to obtain the final current velocity field.

The circles A and B in Figure 8.18 indicate the places on the shore where radar are installed. The angular sectors (dashed lines) indicate the sea surface area covered by each of the radar; the arrows indicate currents measured by each of the radar. These measurements should be geometrically composed to obtain the final direction and amplitude of the average current in the area. The angular range covered by an array of radar antennas may be between 90 and 360° degrees. The angular resolution of an individual antenna may be from a few degrees to tens of degrees.

In general, the most frequent wavelengths of ocean waves, which produce the Bragg resonance, are from 5 to 50 m and the phase speeds in deep water range from about 3 to 10 m/s. For deep-water gravity waves, λ_s is given by

$$\lambda_S = \frac{g}{2\pi} T^2 \tag{8.22}$$

where T is the wave period. It follows from Eq. (8.22) that for the above sea wavelengths, the corresponding periods range from 5.7 to 1.8 s.

8.10.1 Example # 1

A real case of a radar installation is presented in Laws (2001) and will be described below. This system operates on four transmitting frequencies 4.8, 6.8, 13.4 and 21.8 MHz in a sequential mode, so that measurements on the four frequencies are done very fast. The transmitted pulse period is adjustable between 10 and 200 μs and establishes the range resolution in about 3 km. As explained before (Section (8.2)), there is a distance where the radar is blind. For this particular system the minimum distance from which information can be usable and currents can be measured is about 6 km from the radar's antenna.

In order to transmit with four frequencies, four power amplifiers with their corresponding antennas would be required. With the purpose of diminishing this number, the system was divided into a low band section operated at 4.8 and 6.8 MHz and a high-band section operated at 13.4 and 21.8 MHz, thus each one requires only one power amplifier. The power amplifier produced a signal pulse of about 50 W, but power can be increased to about 250 W.

Two separate half-wave vertical monopole antennas were used to irradiate the sea surface; each antenna has a resonant filter which permits them to be used to transmit two frequencies. The energy emitted by these antennas are backscattered by the sea waves and received by an array of antenna elements which works as a single directionally variable antenna (Section (3.5.3)). This array permits the direction where the signal comes from to be known. The elapsed time between the moment the pulse was sent and the instant the backscattered signal arrives allows the distance traveled by the signal to be determined.

The array consisted of eight loop antennas placed about 1 m above the ground and disposed aligned along the shoreline over a distance of about 50 meters, and

separated by about 7 m (Fig. 8.19). The time delay between elements of this line of antennas is used to sequentially point the composed antenna at different directions as explained for the technique called beamforming (Section (3.5.3)). Recall that beamforming consists in shifting the phase of the signals coming from the individual antenna elements in such a way that when all the signals from the elements are summed, only those from a given direction will add in phase (Laws, 2001).

Each antenna has it own pre-amplifier and the signals from them are multiplexed and sent to the data processing unit. The radar system works approximately 12 minutes each hour to produce an hourly data file.

A boat with a transponder was used with the aim of calibrating the system. In this case a transponder is a device that emits an electromagnetic signal at a frequency similar to that of the radar. Thus, positioning the boat in known places and emitting signals which simulate those backscattered by the sea it is possible to calculate the amplification and phase shift needed for each antenna in order to properly calibrate the array with the intention that it effectively positions the boat. In other words, corrections were calculated so that the radar determination of the successive transponder positions agrees with the real positions. In the system presented herein the accuracy in the angle determination was estimated in ± 1.5°.

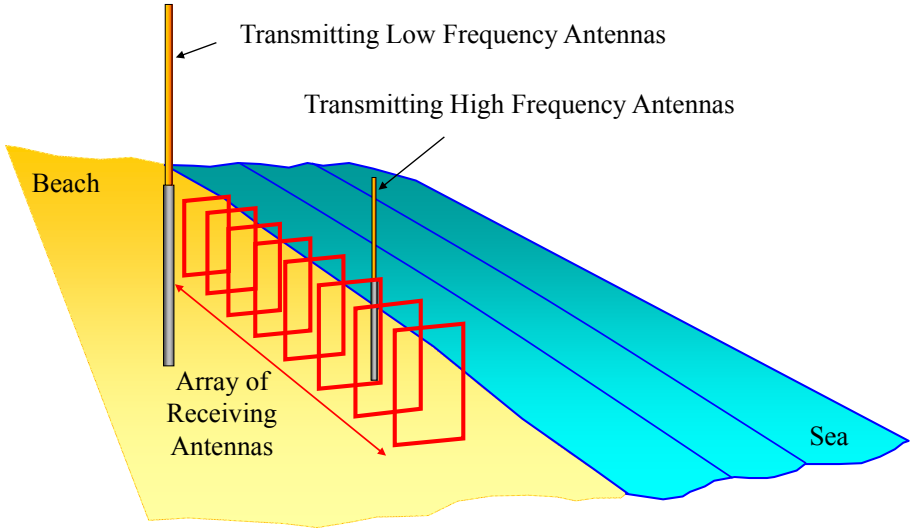

Fig. 8.19: Example of an array of transmitting and receiving antennas for measuring ocean currents (Laws, 2001).

8.10.2 Example # 2

Another radar system called Coastal Ocean Dynamics Applications Radar (CODAR) uses a more compact set of co-located antennas which sweeps the sea surface pointing at different directions. It requires much less space for installation and results easier to transport than the array of antennas previously discussed (Fig. 8.20). Two crossed looped antennas were mounted in orthogonal orientation with a single monopole antenna at the center (Paduan & Rosenfeld, 1996). CODAR operates at about 25 MHz so that the radar wavelength of 12 m resonates with ocean waves 6 m in length. The angular sector covered by the system is 120° and the range extends up to 15 km (Kovacevic et al., 2004). The system provides hourly radial velocities at 5° angular resolution and the data from two or more systems are combined to produce vector current maps with magnitude accuracy of 0.07 m/s and 10 degrees in direction.

Fig. 8.20: Pole with CODAR antennas (Courtesy of Andrea Mazzoldi CNR, Italy).

Some wide radar networks (more than 60 nested systems) to routinely monitor surface current in large areas have been reported (Garfield et al., 2011). In this case, CODAR systems of different characteristics were employed to cover a long coastal area of California, USA. Several 5 MHz systems that have an average range of approximately 180 km and spatial resolution of 6 km were nested with 12 and 25 MHz systems to cover ranges from 40 to 90 km with 1 or 3 km of spatial resolution.

In smaller areas where better spatial resolution is required, smaller networks of higher-frequency CODAR have been employed (Garfield et al., 2011). Four 42 MHz systems with a spatial resolution of 400 m are reported in the San Francisco Bay, California. This radar frequency produces a coherent Bragg scatter with waves of 3.5 m in length. These radar waves perceive the influence of currents to a water depth of 1.8 m and currents can be estimated with an accuracy of about 0.085 m/s. It is expected that with the addition of two CODAR of the same characteristics, the spatial resolution of this array will be increased to 200 m and the angular grid to one degree. It was also estimated that a 30 minute averaging time is adequate to predict currents in almost "real time". This information can be used to assist the racers of a boat competition with surface current information in planning the race strategy (Garfield et al., 2011).

An interesting finding followed the 9.0 magnitude earthquake off Sendai, Japan, on 11 March 2011. Tsunami signals were observed at five HF radar sites installed with the purpose of monitoring surface currents. Radar were installed on different continents and separated by a distance of 8,200 km. Authors report that the expected current flow and velocity oscillations due to the tsunami have been observed in the data from Hokkaido and California a short time before impacting on the shore (Lipa et al., 2011). They conclude that HF radar installations, in some locations where shallow-water bathymetry extends well offshore, could provide capability for the detection of approaching tsunamis.

In summary, the theory and technology of radar systems to monitor ocean dynamics from the shore have evolved quickly in the last 20 years. Radar systems were reduced in size and "in situ" data processing become feasible. At present it is possible to estimate ocean surface currents in wide areas with accuracy better than 0.08 m/s and with grid angular resolution of about one degree. Also, in some cases it seems possible to predict currents in a 30 minute averaging time which, for certain applications may be considered almost "real time". In some particular coast bathymetry it seems a useful tool in the early detection of tsunamis.

8.11 Ground Penetrating Radar (GPR)

It is a technique used to investigate the shallow subsurface of the Earth. It can provide information about the nature and depth of buried objects, and man-made or natural structures. Also, it has proved to be a useful tool in rescuing buried victims after building destructions (Cist, 2009). In addition, this technology has been used to find the ice thickness in the Polar Regions (http://www.sensoft.ca/FAQ.aspx). As in all of the radar already studied it works by emitting an electromagnetic wave and receiving its echoes. The information about the buried objects is derived from the echoes. Two antennas are used in this technique, one to emit and another to receive.

The GPR antennas are placed over the surface of the earth; one of them emits electromagnetic energy into the soil, exactly in the opposite sense to that of the radar

used to profile the wind in the atmosphere (Section (8.6)). For this reason, this method uses principles analogous to those used in the seismic reflection method (Daniels, 2000).

The electromagnetic waves radiated into the subsurface travel at a speed (v), which is a function of the permittivity (ε) of the material. Then the propagation speed is different in materials with different electrical properties. The speed is inversely proportional to the square root of the permittivity times the permeability (μ) of the material (Skilling, 1974),

$$v = \frac{1}{\sqrt{\mu\,\varepsilon}} \tag{8.23}$$

Since the permittivity of earth materials is always greater than the permittivity of air, the speed of a wave in a material other than air is less than 3×10^8 m/s. The time interval required for a wave to travel from the transmitting antenna to the receiving antenna is called the **travel time**.

Let us consider the transmitting and receiving antennas placed as in Figure 8.21. In real instruments, both antennas are mounted on a trolley that permits them to be displaced on the Earth surface keeping their relative distance constant. When a pulse is radiated by the transmitting antenna (T_A), the receiving antenna (R_A) will receive first a pulse which traveled directly through the air (D). After some delay other pulses (R) will be received by the antenna; these correspond to waves reflected or scattered by subsurface objects. They travel through the material and arrive back at the surface. These pulses travel at a velocity determined by the permittivity (ε) of the soil material.

The reflections and scatterings of the single pulse sent from the transmitting antenna produce a sequence of pulses arriving at the receiving antenna that correspond to all the different echoes (travel paths). The recording of these pulses is called a **trace** and it is shown in Figure 8.22 for the example of Figure 8.21.

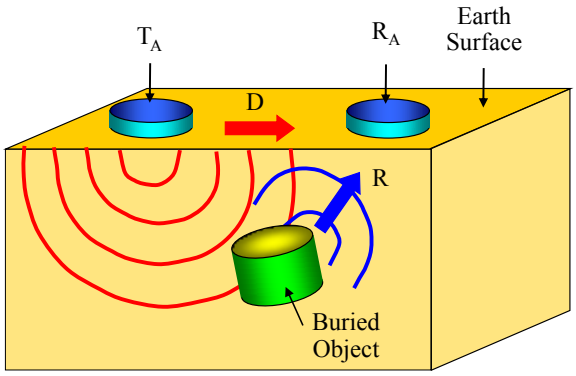

Fig. 8.21: A pulse is radiated by the transmitting antenna (T_A); the receiving antenna (R_A) will collect pulses (D) and (R). The first travels directly through the air; the second corresponds to waves reflected or scattered by subsurface objects.

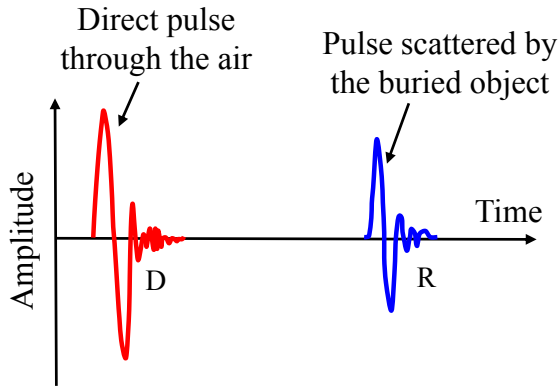

Fig. 8.22: Pulses arriving at the receiving antenna produce a time-dependent record called a trace.

The received pulses have different amplitudes and arrive with different delays; delays are greater for farther buried objects. If the propagation speed of the wave in the subsurface medium is known, delays can be used to estimate the depth of the scattering objects.

Assume that the subsurface material is homogeneous and that only one object of different permittivity is buried in it (Fig. 8.23). Displacing both antennas together on the surface from position P_1 to P_5 permits the object to be "viewed" from different directions. Because the electromagnetic wave travels downwards traces are usually drawn from above to below (Fig. 8.24a).

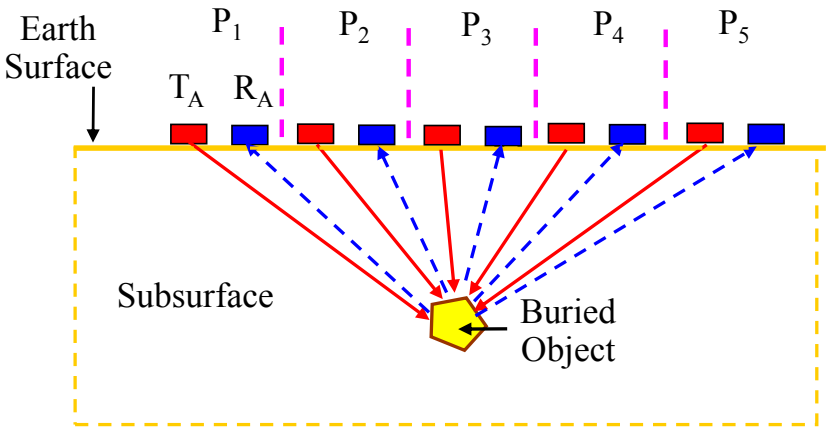

Fig. 8.23: TA and **RA** are at a fixed relative distance and are displaced from position P_1 to P_5. At each position a pulse is emitted and its scatter from the buried object is recorded

Drawing the traces for each position, and ignoring the direct pulse through the air, will produce a picture as shown in Figure 8.24a. The amplitudes of the recorded pulses are larger and have a lesser delay when the GPR is closer to the scattering object (position P_3). Pulses may be transformed in a gray scale ranging from white to black. Black is assigned to the maximum amplitude and white to non reflection. A trace to which this gray scale has been applied is called a **scan**. The scans for these traces are drawn in Figure 8.24b.

The GPR scans form an image of the subsurface where the horizontal axis is the surface position of the antennas and the downward axis is the round-trip travel time of the electromagnetic wave. This record is very similar to that of an acoustic fish finder. The buried object is represented as a vertical parabola or a figure with the shape of an inverted V. The closest approach of the GPR to the buried object occurs at the peak of the inverted V.

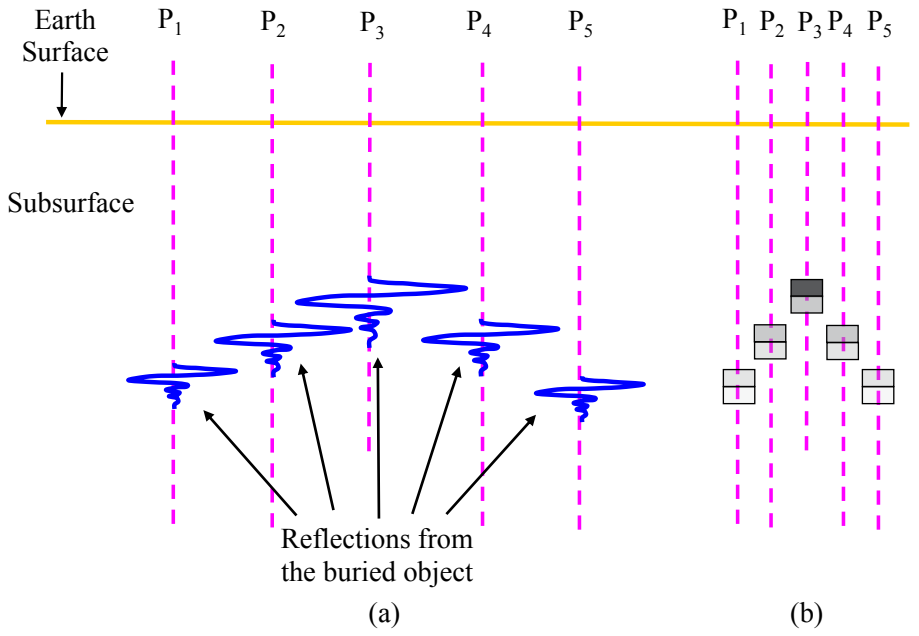

Fig. 8.24: (a) Traces from the buried object. (b) Scans from the buried object.

The electromagnetic wave amplitude decreases exponentially with the distance from the emitting antenna, their scatters becoming undetectable at some point. The attenuation coefficient increases with the electrical conductivity of the material and also with frequency. Then, using radar with lower frequency increases wave penetration into soil, but the price is a loss of spatial resolution.

Radio waves penetrate a few centimeters in sea water, some tens of meters in fresh water and some hundreds of meters in ice (www.sensoft.ca/FAQ.aspx). An approximate way of estimating the exploration depth of a GPR in a given material is by using the approximation of Eq. (8.24), where D is the penetration in meters and σ is the conductivity of the medium expressed in mS/m (www.sensoft.ca/FAQ.aspx).

$$D(m) = \frac{35}{\sigma} \tag{8.24}$$

GPR systems have microprocessor circuits which provide some degree of digital control and allow digital data recording for its post-processing.

So far the GPR has been trolled following only a line, but if it is moved following parallel lines a three dimensional figure of the subsurface can be plotted. The accurate location of each trace is critical for producing reliable 3D pictures. Generally 3D images are constructed from several parallel two dimensional scans as shown on Figure 8.24b.

References

Bahl, M., Gupta, B., John, T., Singh, D., Sharma, O., Garg, S., & Khanna, R. (2011). A phased array acoustic wind profiler for remote atmospheric wind measurements. *IETE Journal of Research*, *57* (2), 190-196. doi:10.4103/0377-2063.81738

Bao, X., Webb, D. J., & Jackson, D. A. (1993) 32-km distributed temperature sensor based on Brillouin loss in an optical fiber. *Optics Letters*, *18* (18), 1561-1563.

Campbell J.B. (2008). *Introduction to Remote Sensing*. New York: The Guilford Press.

Cariou, J. P. & M. Boquet, M. (2011). *LEOSPHERE Pulsed Lidar Principles, Contribution to UpWind WP6 on Remote Sensing Devices*. LEOSPHERE, Orsay, FR pp. 32. Available at: http://www.upwind.eu/media/576/D6.1.1.pdf

Chandrasekhar Sarma T. V., Narayana Rao, D., Furumoto, J., & Tsuda, T. (2008). Development of radio acoustic sounding system (RASS) with Gadanki MST radar – first results. *Annales Geophysicae*, *26*, 2531–2542.

Cist, D. B. (2009). *Non-Destructive Evaluation after Destruction: Using Ground Penetrating Radar for Search and Rescue*. Geophysical Survey Systems Inc., Salem, NH, USA. Non-Destructive Testing in Civil Engineering, Nantes, France.

Coulter, R. (2005). *Radar Wind Profiler and RASS (RWP915) Handbook*. ARM TR-044 U.S. Department of Energy, Office of Science, Office of Biological and Environmental Research.

Daniels, J. J. (2000). *Ground Penetrating Radar Fundamentals*. Department of Geological Sciences, the Ohio State University. Available at: http://www.earthsciences.osu.edu/~jeff/Library/BASICS.PDF

Dean, R. G., & Dalrymple, R. A. (1984). *Water Wave Mechanics for Engineers and Scientists*. Englewood Cliffs, New Jersey: Prentice-Hall, Inc.

DeTect, Inc. (2009). *Radar Wind Profiler Specifications Explained*. Meteorological Systems Group, DeTect Inc Longmont, CO. Document No: 9000190 Availabale at: www.detect-inc.com

Dibbern, J., Engelbart, D., Goersdorf, U., Latham, N., Lehmann, V., Nash, J., Oakley, T., Richner, H., & Steinhagen, H. (2003). *Operational Aspects of Wind Profiler Radars, Instruments and Observing Methods*. Report no 79, World Meteorological Organization. WMO/TD no 1196.

Garfield, N., Hubbard, M., & Pettigrew, J. (2011). Providing SeaSonde High-Resolution Surface Currents for the America's Cup. *Proceedings of IEEE/OES Current, Waves, and Turbulence Measurement Conference, Monterey, CA*. March 20-23, 2011.

Gustafsson, D. (2008). *Remote wind speed sensing for site assessment and normal year correction*. Master of Science Thesis in Energy Technology, KTH School of Industrial Engineering and Management, Department of Energy Technology, Stockholm, Sweden.

Hahn, D. W. (2007). *Raman Scattering Theory*. Department of Mechanical and Aerospace Engineering, University of Florida (USA). Available at: http://plaza.ufl.edu/dwhahn/Raman%20Scattering%20Theory.pdf

Hausner, M. B., Suarez, F., Glander, K. E., et al. (2011). Calibrating Single-Ended Fiber-Optic Raman Spectra Distributed Temperature Sensing Data. *Sensors*, *11*, 10859-10879. doi: 10.3390/s111110859

Hennemuth, B., Peters, G., & Kirtzel, H. J. (2012). Temperature profiles with bi-static Doppler-RASS and their correction. *Atmospheric Measurement Techniques and Discussions*, *5*, 1399-1408.

Hunter, S. M. (2009). Radar Rainfall Estimation: Capabilities, Limitations and Potential Improvements. WSR-88D. National Weather Service Weather Forecast Office (NOAA) Available at: http://www.srh.noaa.gov/mrx/research/precip/precip.php

Jenkins, F. A., & White, H. E. (1957). *Fundamentals of Optics*. New York: McGraw-Hill Book Company.

Jørgensen, H. E., & I. Antoniou, I. (2002). *Inter comparison of two commercially available SODARS*. Risø National Laboratory, Roskilde, Danmark, Risø-R-1383(EN): Pitney Bowes Management Services Danmark A/S.

Kartashov, V. M., Babkin, S. I., & Volokh, A. V. (2008). Analysis of Current Status of Theory and Practice of Radio-acoustic Sounding Systems. *14th International Symposium for the Advancement of Boundary Layer Remote Sensing, IOP Conf. Series: Earth and Environmental Science* **1** 012052. doi:10.1088/1755-1307/1/1/012052

Kinsman, B. (1965). *Wind Waves*. Englewood Cliffs, New Jersey: Prentice-Hall, Inc.

Kovacevic,V., Gacic, M., Mancero Mosquera, I., Mazzoldi, A., & Martinetti, S. (2004). HF radar observations in the northern Adriatic: surface current field in front of the Venetian Lagoon. *Journal of Marine Systems, 51*, 95-122.

Laws, K. (2001). *Measurements of Near Surface Ocean Currents Using HF Radar*. A dissertation submitted in partial satisfaction of the requirements for the degree of Doctor of Philosophy in Physics, University of California, Santa Cruz.

Lillesand, T., Kiefer, R. W., & Chipman, J. W. (2004). *Remote sensing and image interpretation*. New York: John Wiley & Sons.

Lipa B., Barrick, D., Saitoh, S. I., Ishikawa, Y., Awaji, T., Largier, J., & Garfield, N. (2011). Japan Tsunami Current Flows Observed by HF Radars on Two Continents. *Remote Sensing*, *3*, 1663-1679. Available at: www.mdpi.com/journal/remotesensing

Minardo A. (2003). *Fiber-optic distributed strain/temperature sensors based on stimulated Brillouin scattering*. Dottorato di Ricerca in Ingegneria Elettronica, Seconda Universita' Degli Studi Di Napoli, Naples, Italy. Available at: http://www.dii.unina2.it/opto/publications/PhD_Thesis_Minardo.pdf

Mushore, T. D. (2012). *Gauges measurements and ground-radar observation of rainfall over the Water Board district Reggge and Dinkel*. Thesis submitted to the Faculty of Geo-Information Science and Earth Observation of the University of Twente. Enshede, The Netherlands.

Paduan J. D., & Rosenfeld L. K. (1996). Remotely sensed surface currents in Monterey Bay from shore-based HF radar (Coastal Ocean Dynamics Application Radar). *Journal of Geophysical Research*, *101* (C9), 20,669-20,686.

Pant, G. B., Joshi, R. R., Damle, S. H., Deshpande, S. M., Singh, N., Vashistha, R. D., Neekhra, P., Chande, J. V., Kulkarni, A. A., & J. S. Pillai, J. S. (2005). Wind profiler and radio acoustic sounding system at IMD, Pune: Some preliminary results. *Current Science*, *88* (5), 761-769.

Piccolo, F., & Chirico, G. B. (2005). Sampling errors in rainfall measurements by weather radar. *Advances in Geosciences*, *2*, 151–155.

Rocadembosch, F., Sicard, M., Comerón, A., Rodriguez, A., Muñoz, C., López, M., García, D., & Agishev, R. (2003). Remote sensing mediante lidar en la UPC. *Rama de estudiantes del IEEE de Barcelona, Burán*, *20*, 21-26.

Selker J. S., Thévenaz, L., H. Huwald, H., Mallet, A., Luxemburg, W., van de Giesen, N., Stejskal, M., Zeman, J., Westhoff, M., & Parlange, M. B. (2006). Distributed fiber-optic temperature sensing for hydrologic systems. *Water Resources Research*, *42,* W12202. doi: 10.1029/2006WR005326.

Skilling, H. H. (1974). *Fundamentals of Electric Waves*. Huntington, New York: R.E. Krieger Publishing Company.

Sorensen, R.M. (1993). *Basic Wave Mechanics: for Coastal and Ocean Engineers*. New York: John Wiley & Sons, Inc.

Suárez, F., Aravena, J. E., Hausner, M. B., Childress, A. E., & Tyler, S. W. (2011), Assessment of a vertical high-resolution distributed-temperature sensing system in a shallow thermohaline environment. *Hydrology and Earth System Sciences, 15*, 1081-1093. doi:10.5194/hess-15-1081

US EPA (US Environmental Protection Agency) (2000). *Meteorological Monitoring Guidance for Regulatory Modeling Applications*. EPA-454/R-99-005, United States Environmental Protection Agency, Office of Air Quality Planning and Standards,

van de Giesen, N., Steele-Dunne, S. C., Jansen, J., Hoes, O., Hausner, M. B., Tyler, S., & Selker, J. (2012). Double-Ended Calibration of Fiber-Optic Raman Spectra Distributed Temperature Sensing Data, Sensors, 12, 5471-5485. doi: 10.3390/s120505471

World Meteorological Organization. (2008). Guide to Meteorological Instruments and Methods of Observation., WMO-No. 8 (seventh edition).

http://www.sumitomoelectricusa.com/images/stories/opthermo/ftr3000_e.pdf

http://www.sodar.com/about_sodar.htm, acceded November 2012.

http://www.leosphere.com/products2.php?rubrique=169&cat=wl&item=200sfs

https://docs.google.com/viewer?a=v&q=cache:d9CID27DWkkJ:www.tropmet.res.in/~wprass/Chande-lec.ppt+Radio+Acoustic+Sounding+System&hl=es-419&gl=ar&pid=bl&srcid=ADGEEShoy_yESOfuyqvnOUJ9rTUeTw4SVG7mAzqIrSEs_uZtIrakC4BD_qS1w1dpSgHS0JpWn-tam46zhYMVyaj8HRh_XTbWeXXUmXqZvMESKGFrsBAkA6KC589WGT0_xCOZYJobZhqsh&sig=AHIEtbSBtSSM320I8-sxDKWpFND4L3Iq-Q

http://www.leosphere.com/products2.php?rubrique=157&cat=wl&item=wc200fs

http://www.sensoft.ca/FAQ.aspx

http://www.bom.gov.au/australia/radar/about/what_is_radar.shtml